Role of Charged Residues in the S1–S4 Voltage Sensor of BK Channels

Zhongming Ma, Xing Jian Lou, and Frank T. Horrigan

Department of Physiology, University of Pennsylvania School of Medicine, Philadelphia, PA 19104

The activation of large conductance Ca^{2+}-activated (BK) potassium channels is weakly voltage dependent compared to Shaker and other voltage-gated K^+ (K_V) channels. Yet BK and K_V channels share many conserved charged residues in transmembrane segments S1–S4. We mutated these residues individually in mSlo1 BK channels to determine their role in voltage gating, and characterized the voltage dependence of steady-state activation (P_o) and I_K kinetics ($\tau(I_K)$) over an extended voltage range in 0–50 μM $[Ca^{2+}]_i$. mSlo1 contains several positively charged arginines in S4, but only one (R213) together with residues in S2 (D153, R167) and S3 (D186) are potentially voltage sensing based on the ability of charge-altering mutations to reduce the maximal voltage dependence of P_O. The voltage dependence of P_O and $\tau(I_K)$ at extreme negative potentials was also reduced, implying that the closed–open conformational change and voltage sensor activation share a common source of gating charge. Although the position of charged residues in the BK and K_V channel sequence appears conserved, the distribution of voltage-sensing residues is not. Thus the weak voltage dependence of BK channel activation does not merely reflect a lack of charge but likely differences with respect to K_V channels in the position and movement of charged residues within the electric field. Although mutation of most sites in S1–S4 did not reduce gating charge, they often altered the equilibrium constant for voltage sensor activation. In particular, neutralization of R207 or R210 in S4 stabilizes the activated state by 3–7 kcal mol^{-1}, indicating a strong contribution of non–voltage-sensing residues to channel function, consistent with their participation in state-dependent salt bridge interactions. Mutations in S4 and S3 (R210E, D186A, and E180A) also unexpectedly weakened the allosteric coupling of voltage sensor activation to channel opening. The implications of our findings for BK channel voltage gating and general mechanisms of voltage sensor activation are discussed.

INTRODUCTION

To sense voltage, ion channels must contain charged residues whose position in the membrane electric field change upon voltage sensor activation. Identifying these residues and their contributions to voltage sensitivity are critical to understanding the gating of any voltage-dependent channel. Voltage-dependent K^+ channels share a common "core" architecture, including six transmembrane segments (S1–S6) with an S1–S4 voltage sensor and S5–S6 pore domain in each subunit (Fig. 1 A). Many conserved basic and acidic amino acids are present in S1–S4 that could potentially contribute to voltage sensing (Fig. 1 B). However, in Shaker, only four residues in S4 and one in S2 account for the majority of gating charge (Fig. 1 B, double starred positions) (Aggarwal and MacKinnon, 1996; Seoh et al., 1996). That a few charged residues make large contributions to voltage sensitivity is supported by evidence in Shaker (Larsson et al., 1996; Starace and Bezanilla, 2001), hERG (Zhang et al., 2004), and Na^+ channels (Yang et al., 1996) that the accessibility of S4 positions to internal and external solutions can switch sides upon voltage sensor activation, implying that some charges traverse the entire electric field. Although the majority of charged residues in S1–S4 appear to be non–voltage sensing, their conservation suggests they also play important roles in channel structure or function. Salt bridge interactions between oppositely charged amino acid side chains in different transmembrane segments, including non–voltage-sensing residues, are observed in the crystal structures of KvAP (Jiang et al., 2003) and Kv1.2 (Long et al., 2005a), and impact Shaker biogenesis (Papazian et al., 1995; Tiwari-Woodruff et al., 1997). Non–voltage-sensing residues also influence channel gating, suggesting they participate in interactions that depend on the activation state of the voltage sensor (Tiwari-Woodruff et al., 2000).

Large conductance Ca^{2+}-activated (BK) channels (Slo1) exhibit a pattern of charged residues in S1–S4, similar to that of Shaker and other strongly voltage-dependent K (K_v) channels (Fig. 1 B). However, an equivalent of only 2.6 e per channel are estimated to traverse the electric field upon activation of mSlo1 (Horrigan and Aldrich, 1999), a fivefold smaller gating charge than Shaker (13 e) (Aggarwal and MacKinnon, 1996; Seoh et al., 1996). The molecular basis for this marked difference in voltage sensitivity is unclear. Slo1

Abbreviations used in this paper: BK, large conductance Ca^{2+}-activated; MES, methanesulfonic acid; WT, wild-type.

channels are Ca^{2+} sensitive; but Ca^{2+} acts independent of voltage and has no effect on gating charge (Horrigan and Aldrich, 2002). Slo1 lacks two of the five most important voltage-sensing residues in Shaker (Fig. 1 B), including one in S4; but this difference seems insufficient to account for a fivefold reduction in gating charge. Slo1 retains a series of three regularly spaced arginines in S4 that match key voltage-sensing residues in Shaker even when alternative alignments are considered (Diaz et al., 1998). Moreover, the pattern of arginines in the NH$_2$-terminal half of S4 in Slo1 appears identical to that of Kv2.1 (Fig. 1 B), which exhibits a gating charge similar to that of Shaker (Islas and Sigworth, 1999).

Several mechanisms could account for the relatively weak voltage dependence of BK channel activation. First, voltage sensor movement in Slo1 may be limited compared with Shaker, such that the number of voltage-sensing positions is reduced and/or each residue makes a smaller contribution to gating charge. A reduced contribution of individual residues seems likely, since even one S4 arginine traversing the entire electric field, as in Shaker, should exceed the total gating charge of mSlo1. Alternatively, S4 residues could make large contributions to gating charge if additional sites make contributions of opposite polarity such that the net gating charge is small. Finally, fundamental differences in the structure and/or movement of voltage sensors in BK and K$_V$ channels may exist, such that voltage-sensing residues in Slo1 correspond to non–voltage-sensing positions in Shaker, and the pattern of charge residues is not predictive of differences in voltage sensitivity.

Here we examine the effects on voltage-dependent activation of mutating each charged residue in the S1–S4 segments of mSlo1 to understand their role in channel function, to identify voltage-sensing residues, and to determine why BK channels are weakly voltage dependent. Our results indicate that while many charged residues influenced BK channel gating, only four are potentially voltage sensing, and only one is in S4. Charge neutralization at any of these sites reduces voltage sensitivity but the decreases in gating charge are small ($\leq$0.3 e per subunit). The limited contribution of S4 suggests that voltage sensor movement in BK channels is reduced relative to K$_V$ channels and indicates that charged residues outside of S4 make significant contributions to gating charge. That potential voltage-sensing residues in S2 are not in the same location for mSlo1 and Shaker suggests that additional differences exist in the movement or conformation of voltage sensors in these channels. Thus several factors may contribute to the weak voltage dependence of BK channel activation. In addition, our results show that non–voltage-sensing residues make important contributions to voltage gating, in some cases influencing the energetic coupling of voltage sensor activation to channel opening, in others
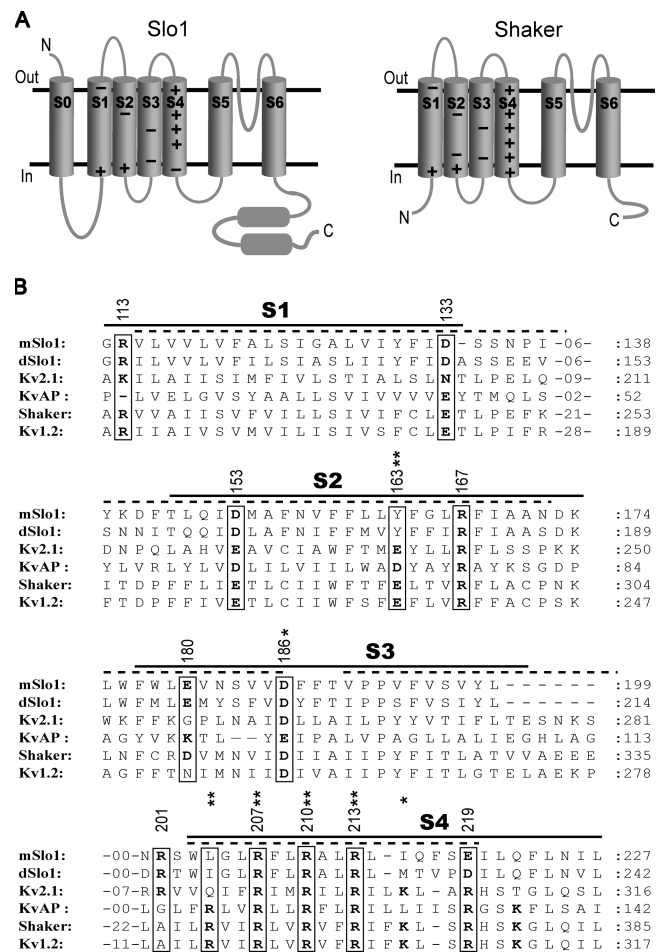
Figure 1. Charged residues in the transmembrane segments of BK and K$_V$ channels. (A) The membrane topology of Slo1 and Shaker potassium channel subunits. Both contain a core domain including S1–S4 voltage sensor and S5–S6 pore. Slo1 contains an additional NH$_2$-terminal transmembrane segment (S0) and large COOH-terminal tail. Conserved basic (+) and acidic (−) amino acids in the S1–S4 segments are indicated. (B) Multiple sequence alignment of voltage sensor domain from mouse and *Drosophila* homologues of Slo1 (mSlo1, dSlo1) and K$_V$ channels (K$_V$2.1, K$_V$AP, Shaker, K$_V$1.2) based on Jiang et al. (2003). Putative transmembrane segments are denoted by solid lines based on hydropathy analysis of Slo1 (Wallner et al., 1996) and dashed lines based on the structure of K$_V$AP (Jiang et al., 2003). Charged residues that are highly conserved in Slo1 or in K$_V$ channels are bold. Positions that were mutated in mSlo1 are numbered and indicated by boxes. Potential voltage-sensing residues in Shaker are indicated by stars, with double stars indicating those where mutation has the greatest impact on gating charge (Aggarwal and MacKinnon, 1996; Seoh et al., 1996).

profoundly influencing the equilibrium constant for voltage sensor activation.

MATERIALS AND METHODS

Channel Expression

Experiments were performed with the mbr5 clone of the mouse homologue of the Slo1 gene (mSlo1) (Butler et al., 1993) expressed in *Xenopus* oocytes. The clone was modified to facilitate

mutagenesis and was propagated and cRNA transcribed as described previously (Cox et al., 1997). Oocytes were injected with ~0.5–50 ng of cRNA, incubated at 18°C, and studied 3–7 d after injection. Site-directed mutagenesis was performed with the QuikChange XL Site-Directed Mutagenesis Kit (Stratagene) and confirmed by sequencing. Some mutants (E180A, D186A, R210N, and E219Q) were provided by J. Cui (Washington University, St Louis, MO).

Electrophysiology and Data Analysis

Currents were recorded using the patch clamp technique in the inside-out or outside-out configuration (Hamill et al., 1981). For I_K measurements, the internal solution contained (in mM) 110 K-methanesulfonic acid (K-MES), 20 HEPES. 40 µM (+)-18-crown-6-tetracarboxylic acid (18C6TA) was added to chelate contaminant Ba^{2+} (Diaz et al., 1996; Neyton, 1996). In addition, "0 Ca^{2+}" solution contained 5 mM EGTA, reducing free Ca^{2+} to an estimated 0.8 nM in the presence of ~10 µM contaminant Ca^{2+}. Solutions containing Ca^{2+} were buffered with 5 mM HEDTA, and free $[Ca^{2+}]$ was measured with a Ca^{2+} electrode (Orion Research Inc.). Nominal $[Ca^{2+}]$ reported as 1, 10, and 50 µM corresponded to measured concentrations of 0.87, 8.7, and 49.9 µM, respectively. Ca^{2+} was added as $CaCl_2$, and $[Cl^-]$ was adjusted to 10 mM with HCl. The external solution contained 110 K-MES, 2 $MgCl_2$, 6 HCl, 20 HEPES. For gating current measurements, the internal solution contained 135 NMDG-MES, 6 NMDG-Cl, 20 HEPES, 2 EGTA, 40 µM 18C6TA. The external solution contained 125 TEA-MES, 2 TEA-Cl, 2 $MgCl_2$, 20 HEPES. The pH of all solutions was adjusted to 7.2 with MES. Experiments were performed at room temperature (20–22°C).

Data were acquired with an Axopatch 200B amplifier (Axon Instruments, Inc.) in patch mode with the Axopatch's filter set at 100 kHz. Currents were subsequently filtered by an 8-pole Bessel filter (Frequency Device, Inc.) at 20 kHz and sampled at 100 kHz with an 18-bit A/D converter (Instrutech ITC-18). A P/4 protocol was used for leak subtraction (Armstrong and Bezanilla, 1974) with a holding potential of −80 mV. For some mutants, with increased P_O, current traces in high $[Ca^{2+}]$ were leak subtracted using a leak trace recorded in 0 Ca^{2+} at $V \leq -140$ mV before and after changing $[Ca^{2+}]_i$. Electrodes were made from thick-walled 1010 glass (World Precision Instruments, Inc.) and their tips coated with wax (KERR Sticky Wax). The electrode's resistance in the bath solution (1.0–2.5 MΩ) was used as an estimate of series of resistance (R_S) for correcting the voltage at which macroscopic I_K was recorded. Series resistance error was <15 mV for all data presented. A Macintosh-based computer system was used in combination with Pulse Control acquisition software (Herrington and Bookman, 1995) and Igor Pro for graphing and data analysis (WaveMetrics, Inc.). A Levenberg-Marquardt algorithm was used to perform nonlinear least-squared fits.

Open probability (P_O) was estimated over a wide voltage range by recording macroscopic I_K when P_O was high (≥ 0.005–0.05), and single channel currents in the same patch when P_O was low (≤ 0.01–0.1). Macroscopic conductance (G_K) was determined from tail currents at −80 mV, following 30-ms voltage pulses, and was normalized by G_{Kmax} measured in 50 µM Ca^{2+} to estimate P_O. At more negative voltages, NP_O was determined from steady-state recordings of 1–60 s duration that were digitally filtered at 5 kHz. NP_O was determined from all-points amplitude histograms by measuring the fraction of time spent (P_K) at each open level (K) using a half-amplitude criteria and summing their contributions. $NP_o = \sum kP_k$. P_o was then determined by estimating N from G_{Kmax} in 50 µM Ca^{2+} (N = G_{Kmax}/g_K, where g_K is the single channel conductance at −80 mV).

Patch to patch variation in the half-activation voltage (V_h) of the G_K-V relationship is observed for Slo1 channels (Stefani et al., 1997; Horrigan et al., 1999) and causes broadening in the averaged voltage-dependent relationships relative to individual experiments. To compensate for such variation, V_h was determined

for each patch and P_o-V relations were shifted along the voltage axis by $\Delta V_h = (<V_h> - V_h)$, where $<V_h>$ is the mean for all experiments at the same $[Ca^{2+}]$, before averaging (Horrigan and Aldrich, 1999; Horrigan et al., 1999).

Mean activation charge displacement ($q_a = kT\ d(\ln(P_O)/dV)$) was measured from the slope of the $\ln(P_O)$-V relation by linear regression over 60-mV intervals (approximately four data points) and plotted against mean voltage. This procedure minimized noise while introducing errors of at most 5% in q_a, based on simulations using the HCA model (Horrigan et al., 1999). Fits of the q_a-V relation by gating schemes were similarly determined by simulating the data at 20-mV intervals and determining q_a by linear regression.

Gating currents were measured using admittance analysis as previously described (Horrigan and Aldrich, 1999). In brief, inside-out patches were excised into nominally K^+-free solutions containing isotonic TEA in the extracellular solution to block residual ionic currents. Currents were recorded in response to 0.5–1-s voltage ramps upon which a sinusoidal voltage command (1736 hz, 60 mV peak to peak) was superimposed. Admittance was calculated for each cycle of the sinwave, and capacitance was determined after correcting for phase shifts due to instrumentation. The voltage-dependent component of the capacitance signal due to gating current was integrated over the voltage range to determine the Q-V relation, which was sampled and plotted at 20-mV intervals. The resulting Q-V is a pseudo steady-state measurement that approximates the closed channel charge distribution (Q_C) at voltages where P_O is small (Horrigan and Aldrich, 1999).

The steady-state data in 0 Ca^{2+} were fit with the HCA model using a semi-automated procedure to estimate the best values and standard deviation for each parameter based on least-squares criteria. After determining the best fit to the $\log(P_o)$-V relation, with all parameters allowed to vary, the parameters were refined by iteratively fitting q_a-V and $\log(P_O)$-V. First the voltage sensor charge (z_J) was varied to fit q_a at voltages where $P_O < 0.1$. Under these conditions, q_a is highly dependent on z_J. $\log(P_O)$-V was then fit with all parameters except z_J allowed to vary. The procedure was repeated until z_J approached a constant value. In this way, reasonable fits were obtained to both $\log(P_O)$ and q_a, and the values of charge (z_J) and coupling (D) were better constrained than by fitting either relation alone. In some cases where gating was shifted to very negative or positive voltages (R207Q,E; R210C; R213C,E; and D153C,K), the coupling factor D was poorly constrained and was held to the wild-type (WT) value until z_J was determined; and then D was allowed to vary with z_J held constant. Data in multiple $[Ca^{2+}]$ were fit by eye using the HA model (see RESULTS).

RESULTS

Mutation of Charged Residues in S1–S4 Alter mSlo1 Gating

To study the role of charged residues in the BK channel voltage sensor, we examined the effects on the voltage dependence of steady-state activation (P_O) and macroscopic kinetics ($\tau(I_K)$) of mutating individual sites in the S1, S2, S3, and S4 segments of mSlo1 indicated in Fig. 1 B. Charged residues were replaced by neutral (A, C, N, Q) or charged (E, K) amino acids to determine the effects of reducing or reversing charge. In addition, a neutral residue in S2 (Y163) was replaced by Glu (E), to match a voltage-sensing position in Shaker (E293). I_K was recorded over a wide voltage range in the virtual absence of internal Ca^{2+} (0 Ca^{2+}, see MATERIALS AND METHODS) to isolate effects of mutation on

voltage-dependent gating from those on Ca^{2+}-dependent mechanisms or the closed to open conformation change (Horrigan and Aldrich, 2002). Measurements were also performed in various $[Ca^{2+}]_i$, including a nearly saturating concentration (50 μM) used to determine the maximal conductance (G_{Kmax}) and estimate the number of channels (N) in each patch to determine P_o (see MATERIALS AND METHODS).

Charge-altering mutations at all sites tested produced functional channels that express macroscopic currents in excised patches. In response to voltage pulses, currents recorded in 0 Ca^{2+} or 50 μM Ca^{2+} activate and deactivate with an approximately exponential time course, qualitatively similar to the WT channel (Fig. 2, A–C). However most mutations in S2, S3, and S4 altered channel gating significantly, as shown in Fig. 2 D by comparing normalized G_K-V relations for WT and mutant channels in 0 Ca^{2+}. Although R207Q, R207E, or R210C in S4 increased P_O relative to the WT and shifted G-V curves to more negative voltages, most mutations inhibited activation. Indeed some mutants appeared almost

nonfunctional in 0 Ca^{2+}, but we were able to characterize their gating properties owing to the high single channel conductance and Ca^{2+} sensitivity of BK channels. For instance, a voltage pulse to +180 mV in 0 Ca^{2+} evoked only single channel currents from a patch expressing R213C channels (Fig. 2 C, left), whereas macroscopic currents are evoked from the same patch in 50 μM Ca^{2+} (Fig. 2 C, right). This shows that hundreds of channels are present and functional, and that P_O in 0 Ca^{2+} is low but measurable based on the resolution of discrete opening events.

The following two sections and Fig. 3 describe the analytical framework used to identify voltage-sensing residues and determine which aspects of channel gating are altered by various mutations. The results of this analysis are summarized in Fig. 4 and Table I.

Identification of Voltage-sensing Residues

Voltage-sensing residues contribute to the total gating charge (z_T) moved in each channel upon voltage sensor activation and channel opening. Therefore, to identify
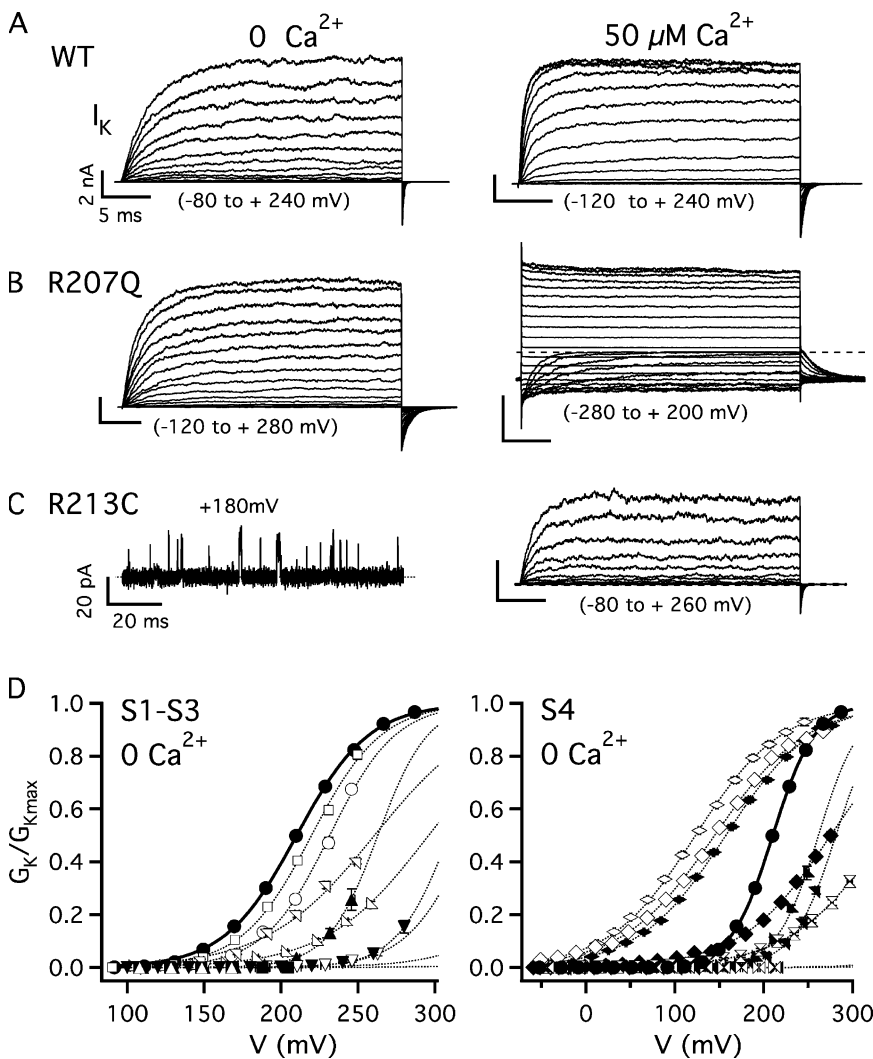

Figure 2. Mutation of charged residues in voltage sensor domain alter mSlo1 gating. Families of I_K evoked from (A) WT (B) R207Q, and (C) R213C channels in response to pulses to different voltages at 20-mV intervals from a holding potential of −80 mV. Currents in 0 Ca^{2+} and 50 μM Ca^{2+} for each channel were recorded from the same patch. Dashed lines indicate the zero current level. (D) G_K-V relations (mean ± SEM) for WT and mutant channels are normalized by G_{Kmax} determined in 50 μM Ca^{2+} and are fit by Boltzmann functions (lines). WT (●), R113Q (○), D133Q (□), D153K (■), D153C (△), Y163E (▲), R167E (▽), R167A (▼), E180A (◣), D186A (◺), R201Q (◤), R207E (◇), R207Q (◆), R210C (◇), R210E (◆), R210N (⊠), R213C (⋈), R213E (⋈), E219Q (◄).

these residues we must determine the impact of charge-altering mutations on z_T. The G_K-V relations in Fig. 2 D are fit by Boltzmann functions, characterized by an apparent charge z_{APP} that was in many cases reduced. However, effects of mutation on z_{APP} are not sufficient evidence that a residue is voltage sensing (Seoh et al., 1996). A more direct indication of gating charge is provided by the mean activation charge displacement q_a, defined in terms of the logarithmic slope of the P_O-V relationship (Sigg and Bezanilla, 1997):

$$ q_a \equiv kT \frac{d(\ln(P_o))}{dV}. \tag{1} $$

For channels that open only when all voltage sensors are activated, q_a increases at negative voltages approach-ing a maximum or limiting slope (q_{alim}) equal to z_T when P_o is small (Almers, 1978; Sigg and Bezanilla, 1997). The limiting slope has been used to estimate z_T for K_V channels (Seoh et al., 1996; Islas and Sigworth, 1999) and Na^+ channels (Hirschberg et al., 1995). However, for BK channels, the relationship between q_a and z_T is more complex because channels can open when no voltage sensors are activated (Horrigan and Aldrich, 2002). The mean P_o-V relation for mSlo1 in 0 Ca^{2+} is plotted on a semilog scale in Fig. 3 A and the corresponding q_a-V relation in Fig. 3 B. At extreme negative voltages (< -100 mV) P_o becomes very small ($\sim 10^{-7}$–10^{-6}) and weakly voltage dependent, exhibiting a limiting slope ($q_{aLim} = 0.3\ e$; Fig. 3 A, dashed line) that represents the small charge associated with channel opening. At more positive voltages, q_a increases to a
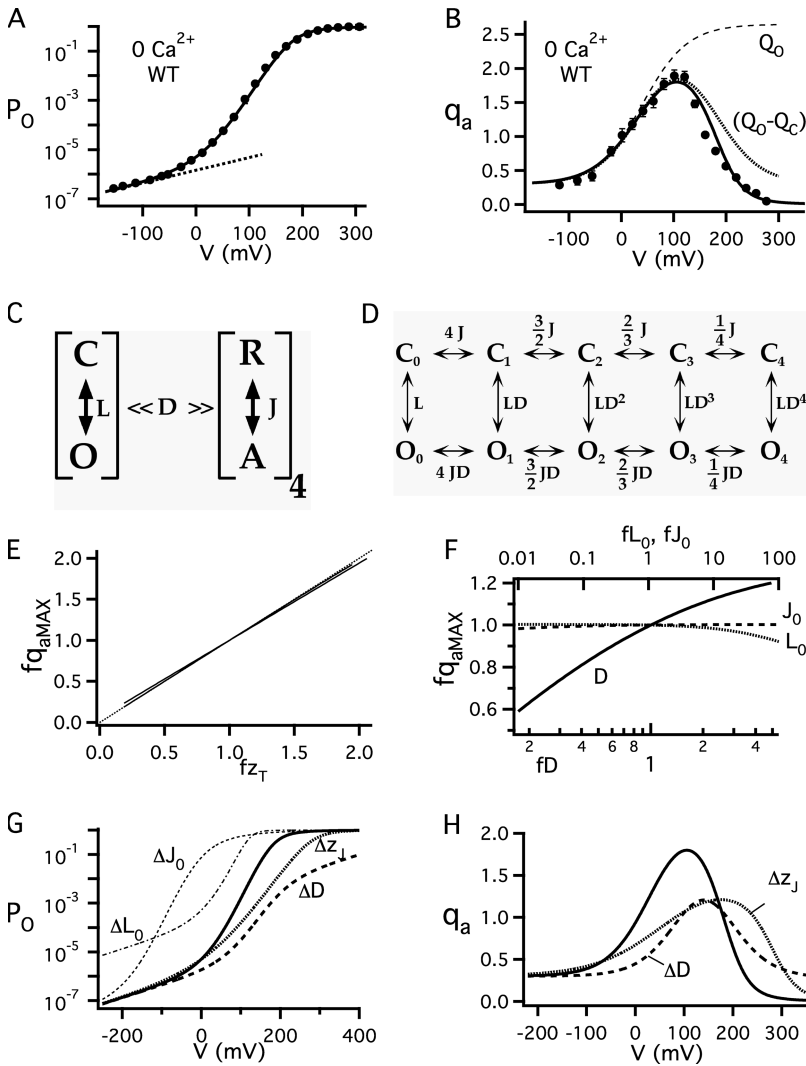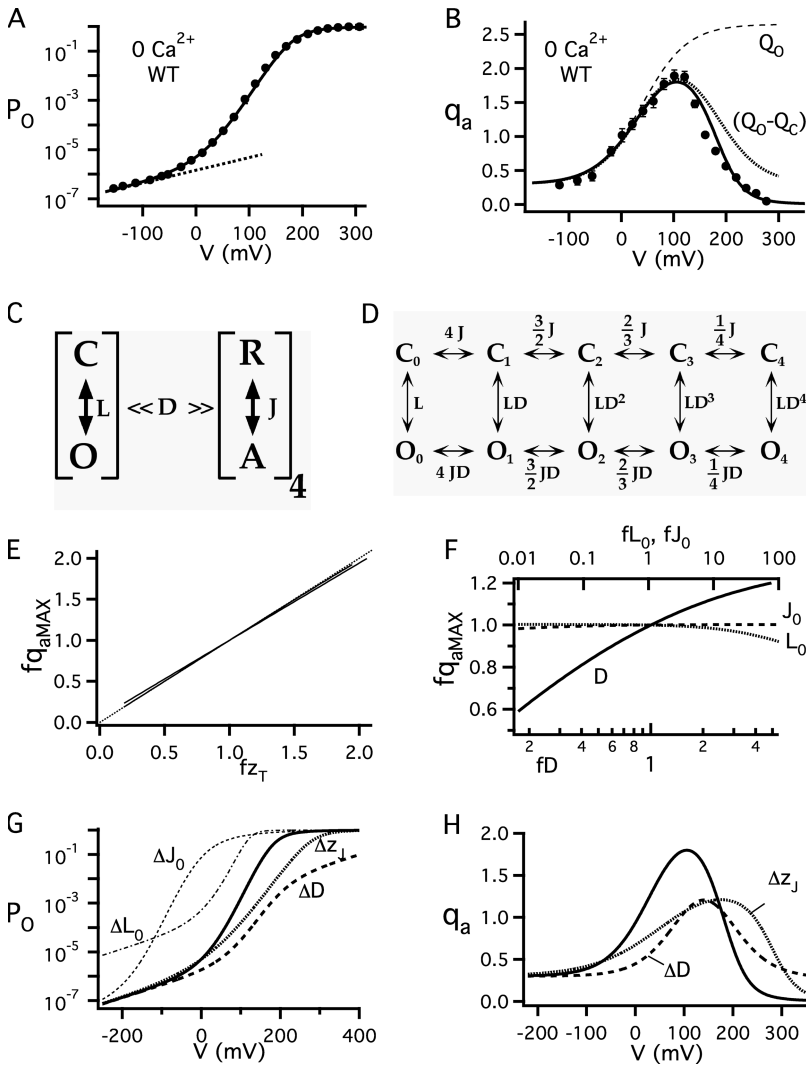

Figure 3. Data analysis and modeling. (A) Po-V relation for WT mSlo1 channels in 0 Ca^{2+} (mean ± SEM) is plotted on a semilog scale and fit by the HCA model (solid line, see be-low). The limiting slope at negative voltages is indicated by a dashed line representing the partial charge associated with channel opening ($z_L = 0.3\ e$). (B) q_a-V relation determined from the logarithmic slope of mean P_O (see MATERIALS AND METHODS). (C) HCA gating mechanism asserts that equilibration of the channel gate between closed and open (C–O) is influenced allosterically by four independent and identical voltage sensors that each can be in a resting or activated state (R–A). The equilibrium constants for channel opening L and voltage sensor activation J are voltage dependent with partial charges z_L and z_J, respectively ($L = L_0 e^{z_L V/kT}, J = J_0 e^{z_J V/kT}$). The activation of each voltage sensor increases the C–O equilibrium constant by an allosteric coupling factor D. (D) Gating scheme shows the closed and open states (C_i, O_i, where i = number of activated voltage sensors) and equilibrium constants specified by the HCA mechanism. Horizontal transitions represent voltage sensor activation, and vertical transitions represent channel opening. Solid lines in A and B represent best fits to the HCA model ($z_J = 0.59\ e$, $z_L = 0.3\ e, J_0 = 0.017, L_o = 1.4 \times 10^{-6}, D = 23.1$) determined by a semi-automated method (see MATERIALS AND METHODS). Dashed lines in B indicate the charge distribution for open channels (Q_O, Eq. 5) and the difference between charge distributions for open and closed channels Q_o – Q_c, Eq. 6), defined by the fit parameters. (E–H) Predicted effects of changing various parameters in the HCA model. (E) Changes in peak q_a, expressed as a fraction of the control value (fq_{aMAX}), produced by changing gating charge (z_J, z_L) are directly proportional to the fractional change in total gating charge (fz_T, where $z_T = z_L + 4z_J$). Dashed line indicates unity slope (b = 1). Solid lines indi-cate effects of proportional changes in both z_L and z_J (b = 0.99) or changing z_J alone (b = 0.94). (F) Effects on fq_{aMAX} of fractional changes in $L_0, J_0,$ or D. (G) Effects on P_O-V relation of changing z_J(0.35 e), D(5.1), J_0(1.7), or L_0(1.4×10^{-4}) and leaving other parameters the same as the WT (solid line). (H) The decreases in z_J or D both decrease q_{aMAX} relative to the WT (solid line) but have distinct effects on the q_a-V relations. In particular, the steepness of the foot of the curve is reduced together with z_J but is not altered by changing D.

Parameters for the HA Model Used To Fit WT and Mutant Data in 0–50 μM Ca^{2+}

	z_J	z_L	z_T	D	$V_{HC}(J)$	J_0	$L_0 \times 10^6$	C
	e	*e*	*e*		mV			
WT	0.58	0.30[a]	2.62	23.9	173	0.0188	1.18	7.0
R113Q	0.59	0.30[c]	2.66	24.0	192	0.0113	0.918	6.5
D133Q	0.56	0.30[c]	2.54	24.0	182	0.0177	0.709	6.5
D153C	0.35	0.17[d]	1.57	23.5	345	0.0084	1.00	6.5
D153K	0.29	0.16[d]	1.32	23.8	435	0.0068	2.95	6.5
Y163E	0.57	0.28[d]	2.56	24.0	262	0.0027	1.39	7.5
R167A	0.46	0.17[d]	2.01	23.8	295	0.0046	1.43	7.0
R167E	0.38	0.18[d]	1.70	22.3	305	0.0101	1.34	7.0
E180A	0.58	0.30[d]	2.62	14.0	148	0.0334	1.25	8.5
D186A	0.36	0.30[d]	1.74	11.9	205	0.0538	2.98	8.5
R201Q	0.59	0.30[c]	2.66	21.0	220	0.0059	1.12	8.0
R207Q	0.57	0.49[b]	2.77	22.5	−105	10.69	0.167	8.5
R207E	0.57	0.56[b]	2.84	21.5	−120	14.99	0.287	7.5
R210C	0.56	0.42[b]	2.66	25.8	−355	2618	0.184	8.0
R210E	0.61	0.33[a, b]	2.77	3.4	25	0.5468	160	7.5
R213C	0.28	0.19[d]	1.31	24.5	475	0.0052	4.05	6.5
R213E	0.24	0.18[d]	1.14	22.5	510	0.0078	3.27	6.5
E219Q	0.56	0.29[d]	2.53	21.9	185	0.0166	0.178	8.0

The HA model (Horrigan and Aldrich, 2002) is an extension of the HCA model (Fig. 3C, D) that accounts for effects of Ca^{2+} and predicts: $P_O = L(1 + KC + JD + JKCDE)^4/[L(1 + KC + JD + JKCDE)^4 + (1 + K + J + JKE)^4]^{-1}$, where $K = [Ca^{2+}]/K_D$, $L = L_0 e^{z_L V/kT}$, and $J = J_0 e^{z_J V/kT}$. In addition to the parameters specified in the HCA model (z_J, J_0, z_L, L_0, D), the HA model includes a Ca^{2+} dissociation constant (K_D) and allosteric factors C and E that describe the interactions of Ca^{2+} binding, at four independent and identical sites, with channel opening and voltage sensor activation, respectively. The value of K_D and E were not well determined by the current data and assumed to be constant with values ($K_D = 11$ μM, E = 2.4) taken from Horrigan and Aldrich (2002), and only C was adjusted to account for the effects of Ca^{2+}. The total gating charge (z_T) and half-activation voltage of the voltage sensor when channels are closed (V_{HC}) are derived from the other parameters ($z_T = z_L + 4z_J$, $V_{HC} = -kT\ln(J_0)/z_J$).
[a]z_L was determined from the weak voltage dependence of P_o at extreme negative voltages.
[b]z_L was determined from the weak voltage dependence of P_o at extreme positive voltages.
[c]z_L was set to the WT value.
[d]z_L was estimated from the voltage dependence of $\tau(I_K)$ at extreme negative voltages according to Eq. 9.

peak ($q_{aMAX} = 1.9 \pm 0.1$ *e*) that reflects voltage sensor activation (Horrigan and Aldrich, 2002).

The relationship between q_a and z_T can be understood based on gating current measurements and some assumptions about voltage gating embodied in a model that accounts for BK channel gating in 0 Ca^{2+} (Fig. 3, C and D) (Horrigan et al., 1999). The HCA model postulates that the transition between the closed (C) and open (O) conformation is influenced allosterically by the state (resting [R] or activated [A]) of four independent and identical voltage sensors (Fig. 3 C). The energetic effect of voltage sensor activation on the C–O equilibrium is represented by a factor D and is fully described in terms of a two-tiered gating scheme (Fig. 3 D) representing the closed and open channel with different numbers (0–4) of activated voltage sensors. The equilibrium constants for the C–O and R–A transitions are both voltage dependent with partial charges z_L and z_J, respectively. Therefore the total gating charge involved in activating all four voltage sensors and opening the channel is $z_T = (4z_J + z_L)$. z_J can be determined from the Q_C-V relation, which is measured from gating current when channels are closed and is well described by a Boltzmann function with a mean charge of $z_J = 0.58$ *e* (Horrigan and Aldrich, 2002). z_L can be determined from the limiting slope $q_{aLim} = 0.3$ *e*. Therefore,

the estimated value of $z_T = 2.62$ *e* exceeds q_a at all voltages (Fig. 3 B). However the HCA model reproduces the P_o-V and q_a-V relations using these estimates of z_J, and z_L (Fig. 3, A and B, solid curves) and therefore reproduces the relationship between z_T and q_a.

In the present study we assessed the impact of mutations on z_T by measuring q_{aMAX}, and by fitting the P_o-V relations in various [Ca^{2+}] with an expanded version of the HCA model that includes the effects of Ca^{2+} (Table I, HA model) (Horrigan and Aldrich, 2002). In principle, z_T could be estimated as for the WT channel, from gating currents and limiting slope. However, the expression of mutant channels was usually insufficient for gating current measurements. On the other hand, moderate levels of channel expression are sufficient to routinely measure the P_O-V relation and q_{aMAX} even at very low P_O, owing to the high single channel conductance of BK channels.

Although q_{aMAX} underestimates the total gating charge, simulations based on the HCA model imply that q_{aMAX} provides a reasonable indicator of changes in z_T. That is, the fractional change in q_{aMAX} for a mutant relative to the WT ($fq_a = q_{aMAX}^M/q_{aMAX}^{WT}$) approximates the fractional change in z_T ($fz_T = z_T^M/z_T^{WT}$) under most conditions. Fig. 3 E plots fq_{aMAX} versus fz_T as charge in the model is altered either by varying z_J alone

or by varying z_J and z_L proportionally (solid lines). In both cases, a linear relationship is observed with a slope near unity, indicating that fq_{aMAX} approximates fz_T over a wide range of gating charge. q_{aMAX} is also sensitive to changes in the allosteric coupling factor D but is virtually unaffected by large changes in the equilibrium constants for voltage sensor activation (J_0) or channel opening (L_0) (Fig. 3 F). Examples of the effects on the P_o-V and q_a-V relations of altering the parameters z_J, L_0, J_0, or D individually are illustrated in Fig. 3 (G and H), respectively.

Distinguishing between Changes in Gating Charge and Allosteric Coupling

Because changes in q_{aMAX} may reflect changes in coupling (D) as well as changes in gating charge (z_J, z_L), it is important that we distinguish between these two possibilities. In general, we were able to determine which parameters in the HA model were altered by fitting the steady-state data (P_O and q_a) over a wide range of conditions. Many of the parameters are highly constrained by subsets of the data at extremes of voltage, $[Ca^{2+}]$, and P_O (Horrigan and Aldrich, 2002). When fitting these data we also focused on several features that depend specifically on coupling or charge. As described below, the magnitude of the P_o increase between extreme positive and negative voltages and the shape of the q_a-V relation provide direct indications of changes in coupling and charge respectively.

Allosteric coupling determines the extent to which the C–O equilibrium constant and P_O is increased by voltage sensor activation (Horrigan et al., 1999). Therefore changes in coupling should alter the magnitude of the P_O increase between extreme negative and positive voltages where voltage sensors are in the resting or activated state, respectively. For the WT channel in 0 Ca^{2+}, P_O increases from a weakly voltage-dependent plateau near 10^{-7} at extreme negative voltages to a level close to unity at voltages (~+300 mV) where the Q-V relation is saturating and voltage sensors are fully activated (Horrigan and Aldrich, 1999). A simulated decrease in gating charge (z_J) that reduces q_{aMAX} by 35% has no effect on the magnitude of the P_O increase between extreme negative and positive voltages (Fig. 3 G, Δz_J). However, a decrease in coupling (D factor) that also reduces q_{aMAX} by 35% greatly inhibits the voltage-dependent P_O increase (Fig. 3 G, ΔD). In this case, P_O fails to approach unity when voltage sensors are fully activated and instead achieves a plateau whose weak voltage dependence, like that at negative voltages, represents the charge associated with channel opening (z_L). Thus, decreases in coupling or charge should have effects on the P_O-V relation that are readily distinguishable, provided the resting and activated states of the voltage sensor are experimentally accessible, and P_o does not saturate before all voltage sensors are activated. Saturation could

result from enhanced coupling (increased D factor) or stabilization of the open state (increased L_0) caused by mutation. Likewise, the presence of Ca^{2+} can obscure changes in coupling by stabilizing the open state.

Changes in gating charge have effects at negative voltages on the voltage dependence of q_a and P_O that are independent of changes in coupling. For any channel with multiple open states the q_a-V relation can be described as a function of P_O and the charge distributions (Q-V relations) for open and closed channels (Horrigan and Aldrich, 2002):

$$q_a = [Q_O - Q_C](1 - P_o). \tag{2}$$

This function can be approximated by the difference of Q_O and Q_C when P_o is small:

$$q_a \cong Q_O - Q_C, \tag{3}$$

when $P_O << 1$.

The relationship between gating charge and q_a defined by Eq. 3 is model independent and analogous to the limiting-slope analysis that has been applied to Shaker and other voltage-gated channels. In general, the shape and magnitude of Q_O-V and Q_C-V relations depend on gating charge, whereas coupling influences only their relative position along the voltage axis (Horrigan and Aldrich, 2002). Thus, Eq. 3 describes a bell-shaped function whose steepness is determined by charge and whose width is influenced by coupling. These properties can be defined exactly in the case of the HCA model, where both Q_O and Q_C are described by Boltzmann functions with identical voltage dependence but different half-activation voltages (V_{HC} and V_{HO}).

$$Q_C = 4z_J \left[1 + e^{-(V - V_{HC})z_J/kT} \right]^{-1},$$

where

$$V_{HC} = -\left[\frac{kT}{z_J} \right] \ln(J_0) \tag{4}$$

$$Q_O = z_L + 4z_J \left[1 + e^{-(V - V_{HO})z_J/kT} \right]^{-1},$$

where

$$V_{HO} = -\left[\frac{kT}{z_J} \right] \ln(DJ_0). \tag{5}$$

Combining Eqs. 3–5 yields an expression for q_a based on the HCA model:

$$q_a \cong z_L + 4z_J \left\{ \begin{array}{l} \left[1 + \left(\tfrac{1}{D} \right) e^{-(V - V_{HC})z_J/kT} \right]^{-1} \\ - \left[1 + e^{-(V - V_{HC})z_J/kT} \right]^{-1} \end{array} \right\} \quad (6)$$

when $P_O \ll 1$.

At extreme negative voltages q_a can be further approximated by Q_O (Eq. 5) (Horrigan and Aldrich, 2002). Fig. 3 B compares the voltage dependence of q_a from the HCA model (solid line) to that of Eqs. 5 and 6 (dashed lines). Eq. 6 provides a good approximation to the q_a-V relation near its peak and at more negative voltages, and therefore helps describe several properties of q_a. First, q_{aMAX} derived from Eq. 6 depends only on gating charge and coupling, as suggested by the simulations in Fig. 3 (E and F):

$$q_{aMAX} = z_L + 4z_J \left[\frac{\sqrt{D} - 1}{\sqrt{D} + 1} \right]. \quad (7)$$

Second, the width of the q_a-V relation is related to the difference in half-activation voltages (ΔV_H) between Q_O and Q_C and will therefore depend on both voltage sensor charge (z_J) and coupling (D):

$$\Delta V_H = V_{HC} - V_{HO} = \left[\frac{kT}{z_J} \right] \ln(D). \quad (8)$$

Importantly, ΔV_H has a reciprocal dependence on z_J and D that is distinct from that of q_{aMAX}. Therefore, decreases in charge or coupling that reduce q_{aMAX} will increase or decrease ΔV_H, respectively, having opposite effects on the width of the q_a-V relation.

Simulations in Fig. 3 H demonstrate that decreases in D or z_J that have identical effects on q_{aMAX} have distinct effects on q_a-V shape. In addition to the opposing effects of D and z_J on q_a-V width, the steepness of q_a-V is altered by gating charge but is independent of coupling. In particular, the foot of the q_a-V relation is well approximated by Q_O (Fig. 3 B) and therefore has a voltage sensitivity that reflects only z_J and a voltage-independent component equal to z_L. In practice, measurements at the foot of the q_a-V relation for many mutants were noisy owing to the small amplitude of the corresponding P_O data. Therefore, to determine z_J, we took the approach of fitting q_a with the HCA model over a broader voltage range that includes q_{aMAX}. However, the fit was restricted to voltages where $P_O < 0.1$, satisfying the simplifying assumption in Eq. 6. In this way, fits depend on coupling as well as charge, but free parameters were limited and their effects could be distinguished based on the above analysis.

Effects of Voltage Sensor Mutations on Gating Charge and Coupling

The effects of individual S1–S4 mutations on gating charge were assessed by comparing fractional changes in the maximal logarithmic slope of the P_O-V relation (q_{aMAX}) (Fig. 4 A) to those in total gating charge (z_T) (Fig. 4 B) and coupling (D) (Fig. 4 C) estimated from fits to the allosteric models. Mutations at six positions in S2 (D153, R167), S3 (E180, D186), and S4 (R210, R213) reduced q_{aMAX} by significantly more than 10%. Four of these (D153, R167, D186, and R213) also reduced z_T and are potentially voltage sensing. Decreases in q_{aMAX} by R210E and E180A appear entirely accounted for by a reduction in the coupling factor D, whereas D186A reduces both charge and coupling.

The total gating charge ($z_T = 4z_J + z_L$) and coupling factor D were estimated by manual and semi-automated fitting protocols with similar results (solid and shaded bars in Fig. 4, B and C). The mean P_O-V, $\log(P_O)$-V, and q_a-V relations in the presence and absence of Ca^{2+} were fit simultaneously using the HA model, with parameters adjusted manually (Table I) to provide the best fit by eye. The charge associated with the closed–open transition (z_L) was additionally constrained by the voltage dependence of $\tau(I_K)$, as described below. The dissociation constant for Ca^{2+} (K_D) and a weak interaction between voltage sensor activation and Ca^{2+} binding (allosteric factor E) have little impact on the determination of z_T or D and were held constant as a simplifying assumption (see Table I legend). Confidence intervals for z_T or D were estimated from the smallest change in z_J (Fig. 4 D) or D (Fig. 4 E) required to exceed the error range (SEM) of P_o. Because data was obtained over a wide range of P_O, V, and $[Ca^{2+}]$, using macroscopic and single channel methods, the parameters were well constrained, but we could not determine a satisfactory method of weighting the different data to allow automated fitting. We were able to fit the 0 Ca^{2+} data using a semi-automated procedure (see MATERIALS AND METHODS) that yielded values of z_T and D (Fig. 4, B and C, shaded bars) consistent with the manual estimates. Based on comparison of the mean and errors bars determined by these two methods a 10% change in z_T or q_{aMAX} or a 20% change in D were deemed significant.

Potential Voltage-sensing Residues in S2, S3, and S4

Steady-state data for mutants at the four potential voltage-sensing sites are compared with that of the WT in Figs. 5 and 6. Mean $\log(P_O)$-V and q_a-V relations for the WT in 0–50 μM Ca^{2+} are plotted in Fig. 5 A and Fig. 6 A, respectively, together with fits to the HA model (solid lines). The corresponding data for R213C, D153K, R167E, and D186A in Fig. 5 (B–E) and Fig. 6 (B–E) are also fit with the HA model (solid lines) and compared with the WT fit (dashed lines). For the purpose of illustration, q_a is shown only in 0 Ca^{2+} and 50 μM Ca^{2+}.
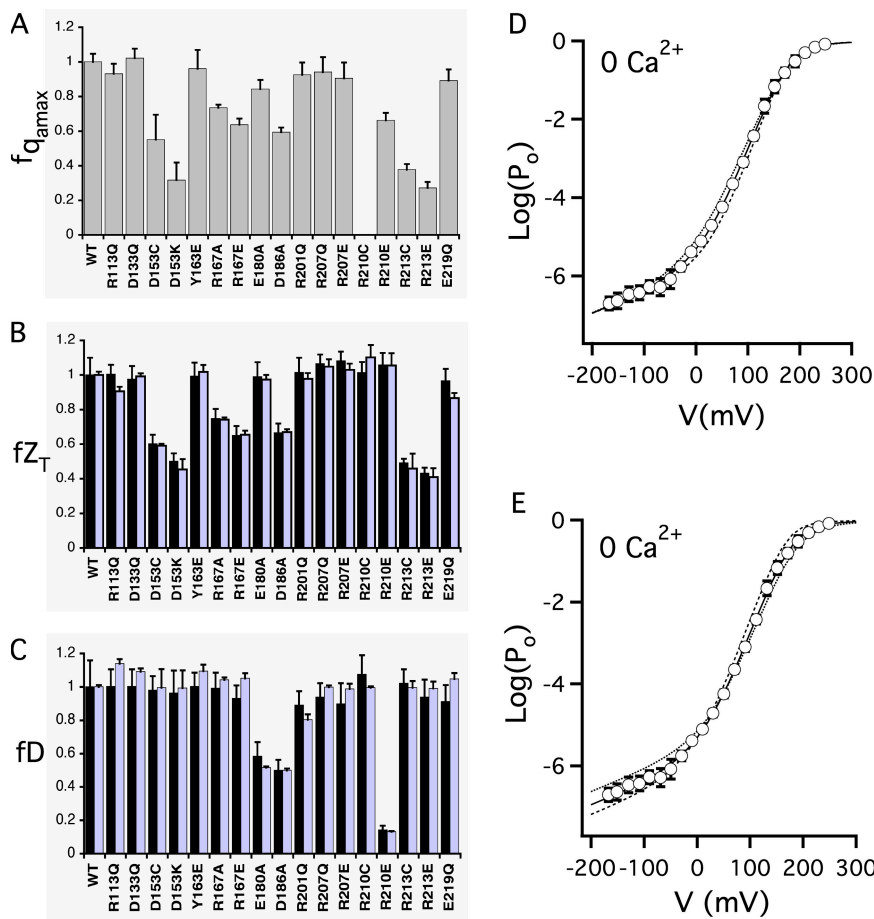
Figure 4. Effects of voltage sensor mutations on gating charge and allosteric coupling. (A) q_{aMAX} for each voltage sensor mutant was determined from the mean P_O-V relation in 0 Ca^{2+} (see MATERIALS AND METHODS) and normalized to that of the WT (1.89 e). q_{aMAX} for R210C could not be determined for reasons discussed in the text. (B) The total gating charge ($z_T = z_L + 4z_J$) and (C) allosteric coupling factor D were estimated from fits of P_O-V and q_a-V relations to the allosteric models and normalized to those for the WT ($z_T = 2.62$ e, D = 23.9). Shaded bars were determined by semi-automated fitting of the HCA model to 0 Ca^{2+} data (see MATERIALS AND METHODS). Solid bars represent fits to data in all [Ca^{2+}] using the HA model (Table I) with parameters adjusted manually. (D and E) Confidence limits for manual fits were estimated for z_T or D by adjusting z_J (panel D) or D (panel E) respectively from the best fit values (solid line) to exceed the error range of P_O as indicated by dashed lines.

However, it is evident from Fig. 5 that the maximal slope of the P_O-V relations (i.e., q_{aMAX}) for mutants were similarly reduced at all [Ca^{2+}]. In addition, mutations increased the width and decreased the steepness of q_a-V relations, consistent with decreases in gating charge (Fig. 6).

The data in Fig. 5 (B–E) and Fig. 6 (B–E) show the effects of a single mutation at each potential voltage-sensing site. At three of these sites (R213, D153, and R167), the effects of both charge neutralization and charge reversal were compared and found to be qualitatively similar (Fig. 4, A–C; Table I). However the effects on z_J of charge reversal were always greater than neutralization (Fig. 5 F; Table I), consistent with these residues acting as voltage sensors. The $\log(P_O)$-V relations in 0 Ca^{2+} for these mutants and the WT are superimposed in Fig. 5 F. Because the q_a-V relation at extreme negative voltages can be approximated by Q_O (Eq. 5; Fig. 3 B), the foot of the $\log(P_O)$-V relation is expected to change shape only if gating charge is altered. In all cases, the mutants in Fig. 5 F show a reduced voltage sensitivity at the most negative voltages, consistent with decreases in gating charge.

The Location of Voltage-sensing Positions in S2

Two of the four potential voltage-sensing residues in mSlo1 are in S2 (D153, R167). K_V channels also contain

conserved acidic and basic residues at these positions (Fig. 1 B). However, the residue corresponding to D153 in Shaker (E283) is non–voltage sensing (Seoh et al., 1996), and the functional role of that corresponding to R167 has not to our knowledge been reported. Shaker does have a potential voltage-sensing residue in S2 (E293) (Seoh et al., 1996) that corresponds to an uncharged residue in Slo1 (Y163) (Fig. 1 B). To determine if this position can sense voltage in mSlo1 we replaced it with the corresponding residue in Shaker (Y163E), but no significant change in q_{aMAX} or z_T was observed (Fig. 4, A and B; Table I). Thus the distribution of voltage-sensing and non–voltage-sensing positions in the S2 of BK and K_V channels appears to be different.

The Voltage Sensor Contributes to Charge Associated with Channel Opening (z_L)

The limiting slope of P_o at negative voltages (q_{alim}) represents the gating charge that moves when channels open (z_L) while voltage sensors are not activated (i.e., C_0–O_0 transition in HCA model; Fig. 3 D). The value of z_L for the WT (0.30 e, Table I) was determined as the slope of mean $\log(P_o)$ from −140 to −280 mV (50 μM Ca^{2+}: $z_L = 0.295 \pm 0.012$ [$n = 10$]; 5 μM Ca^{2+}: $z_L = 0.303 \pm 0.021$ [$n = 3$]) and confirms a previous estimate over a more limited voltage range (Horrigan
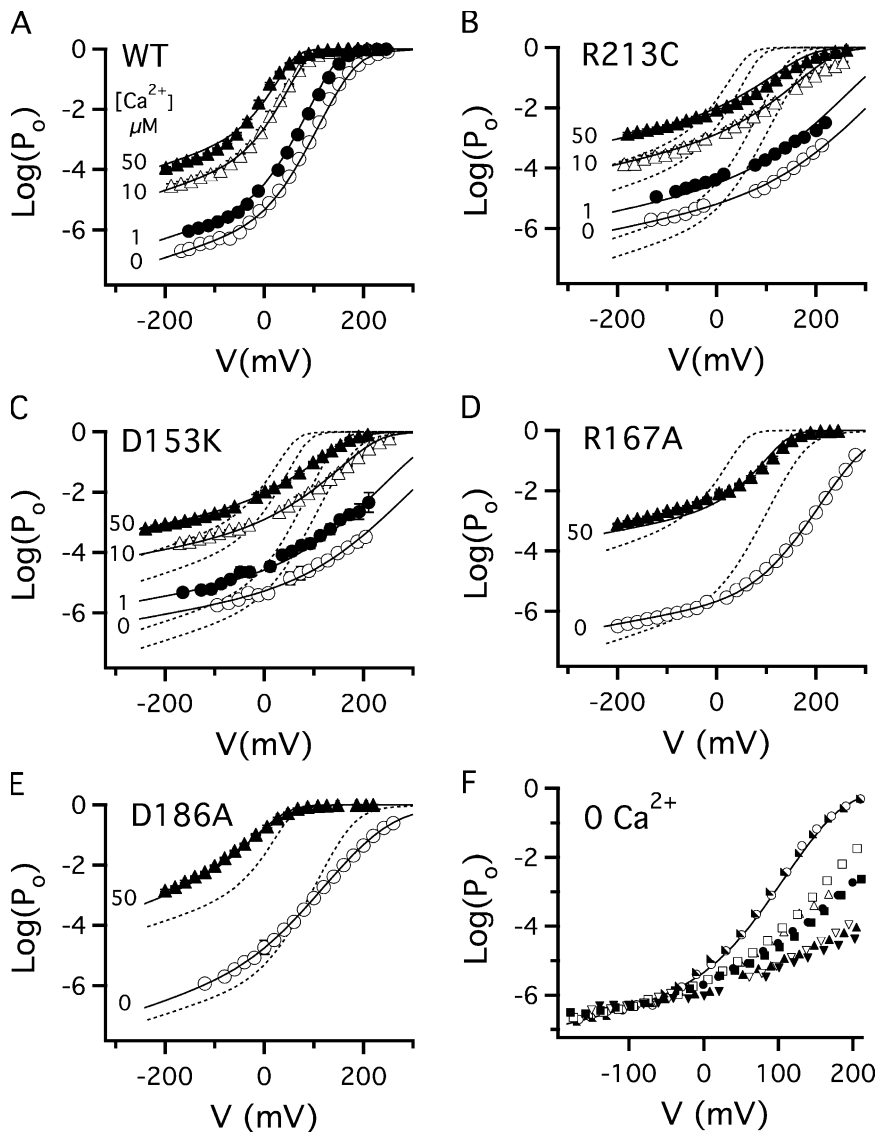
Figure 5. Effect of potential voltage-sensing residue mutations on P_O. Mean $\log(P_O)$-V relations for (A) WT, (B) R213C, (C) D153K, (D) R167A, and (E) D186A in 0–50 μM Ca^{2+}. Solid lines are the fits to the HA model (Table I parameters). Dashed lines represent the WT fit. (F) $\log(P_O)$-V relations in 0 Ca^{2+} for WT (○), D153C(△), D153K (▲), R213C (▽), R213E (▼), R167A (□), R167E (■), D186A(●), and R113Q (◣) are superimposed to show that mutations reduce voltage dependence at the foot of the curve, consistent with a change in gating charge. Mutant curves were shifted along both axes as described below to match the WT at −90 mV. According to analysis presented in the text, the q_a-V relation can be approximated by Q_O (Eq. 5) at extreme negative voltages. Therefore $\ln(P_O)$ can be approximated as the sum of a linear and exponential function: $\ln(P_O) = [\ln(L_0/(1 + L_0)) + (z_L/kT)V] + [4DJ_0\exp(z_JV/kT)]$. Curves were shifted along the voltage axis such that the exponential component of this equation for all curves equaled 0.1 log unit at −90 mV, representing the transition between a linear and nonlinear function (i.e., the foot of the curve). Thus, the voltage shift for mutants was $\Delta V = V_{0.1}(WT) - V_{0.1}(mutant)$ where $V_{0.1} = (kT/z_J)\ln[0.1/(4DJ_0\log(e))]$, and the parameters z_J, D, and J_0 were taken from Table I.

and Aldrich, 2002). z_L is small and could result from subtle changes in the pore domain associated with channel opening, including redistribution of ions and the electric field within the pore (Jiang et al., 2002) or movement of charged residues that are present in S6. However, mutation of potential voltage-sensing residues in S2 (D153, R167) and S4 (R213) reduced z_L (Table I), suggesting that channel opening and voltage sensor activation share a common source of gating charge.

That z_L is reduced by voltage sensor mutation is evident by comparing the q_a-V relations of D153K, R167A, and R213C to that of the WT in 50 μM Ca^{2+} (Fig. 6 F). Over a range of negative voltages, q_a for these mutants is significantly less than the WT value of z_L (dashed line). A decrease in z_L is also obvious by comparing the limiting slope of the P_o-V relations for R167A (Fig. 6 D) to that of the WT fit (dashed lines). By contrast, mutation of a non–voltage-sensing residue (Y163E) shifted

the q_a-V relation to more positive voltages relative to the WT but had no effect on q_{alim} (Fig. 6 F), indicating that z_L was unchanged. In the case of WT and Y163E channels, a limiting value of q_a was clearly achieved over a wide range of negative voltages, allowing z_L to be determined precisely. In general, however, z_L is difficult to determine because at the extreme voltages necessary to measure q_{alim}, steady-state recording for prolonged periods is problematic and P_O is small. Measurement error is minimized in 50 μM Ca^{2+} (e.g., Fig. 6 F) since P_O is increased more than 1,000-fold relative to 0 Ca^{2+} (Horrigan and Aldrich, 2002). However, in some cases, P_O could not be measured at sufficiently negative voltages to achieve a limiting slope (e.g., D186A; Fig. 6 E). More commonly, a limiting slope was achieved or closely approached but could not be measured over a wide enough voltage range to determine z_L within 0.1 e. By contrast, I_K deactivation kinetics can be measured over a much wider range of negative
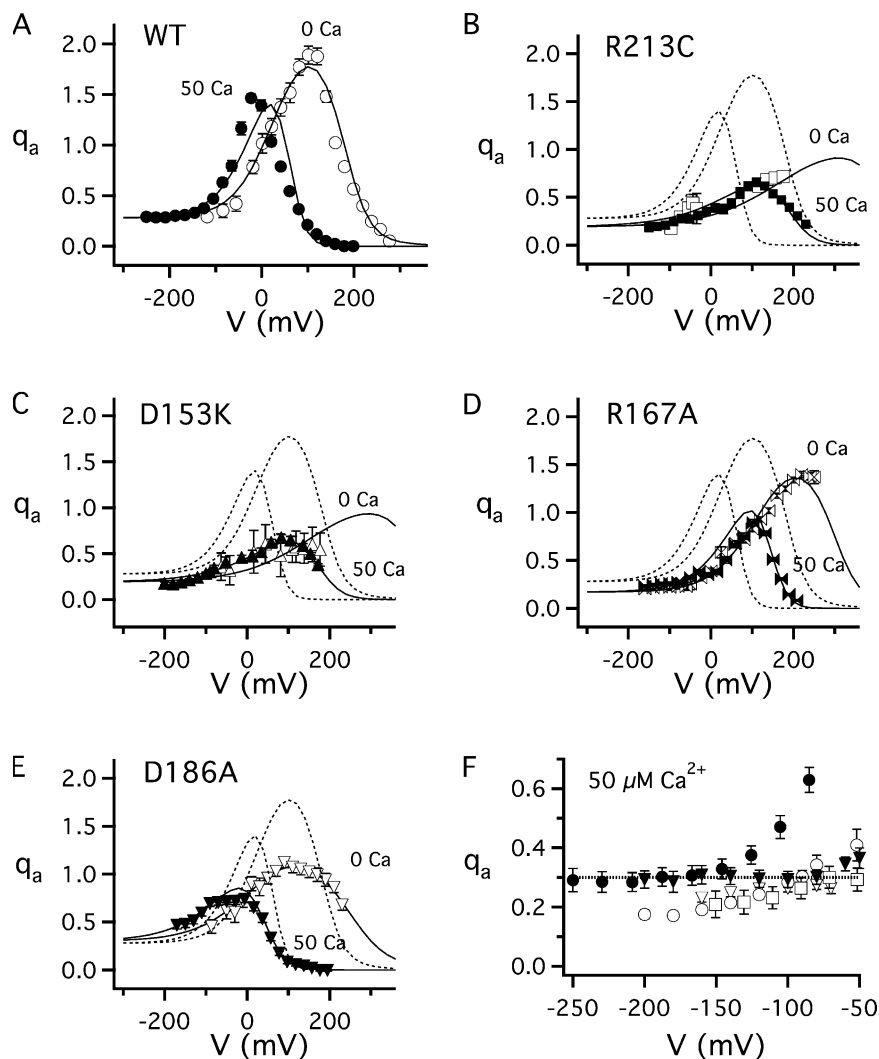
Figure 6. Effect of potential voltage-sensing residue mutations on q_a. Mean q_a-V relations for (A) WT, (B) R213C, (C) D153K, (D) R167A, and (E) D186A in 0 Ca^{2+} and 50 μM Ca^{2+}. Solid lines are the fits to the HA model (Table I parameters). Dashed lines represent the WT fit. (F) Foot of the q_a-V relations in 50 Ca^{2+} for WT (●), Y163E (▼), R213C (□), D153K(○), and R167A (▽) are superimposed to show that the limiting value of q_a (i.e., z_L) is reduced by voltage sensor mutation. Dashed line represents z_L for the WT (0.30 e).

voltages (Horrigan and Aldrich, 2002). Therefore, the voltage dependence of $\tau(I_K)$ (Fig. 7) was used to estimate the values of z_L in Table I.

Macroscopic currents activate or deactivate in response to a voltage step with an exponential time course following a brief delay (Horrigan and Aldrich, 2002). The mean time constants of I_K relaxation ($\tau(I_K)$) for the WT in 0 Ca^{2+} and 50 μM Ca^{2+} are plotted over an extended voltage range in Fig. 7 A. At extreme negative voltages, $\tau(I_K)$ is limited by the rate of channel closing (O_0 to C_0 in the HCA model; Fig. 3 D) and is well fit by an exponential function from -400 to -150 mV (solid lines) whose slope indicates the partial charge (z_N) for closing, and is virtually unaffected by Ca^{2+}. Because z_L represents the sum of z_N and the partial charge for opening, it is likely that z_N will change if z_L is altered. The normalized $\tau(I_K)$-V relations for the WT and several mutants in 50 μM Ca^{2+} are compared in Fig. 7 B at extreme negative voltages. The slopes of such relations were in many cases indistinguishable from that of the WT (z_N; Fig. 7 C). However, mutation of potential volt-

age-sensing residues (R213, D153, and R167) significantly reduce z_N (P < 0.0001; Fig. 7 C), consistent with decreases in z_L.

Because z_N is easier to determine than the limiting slope of P_O, z_L for mutants (Table I) were usually estimated based on the fractional change in z_N relative to the WT:

$$z_L(\text{mutant}) = z_L(\text{WT})\,[z_N(\text{mutant})/z_N(\text{WT})]. \quad (9)$$

A priori, the ratio of z_N to z_L need not remain constant. However, z_N and q_{aLim} were well correlated (r = 0.96) in cases where both were determined (Fig. 7 C), implying that Eq. 9 is a reasonable approximation. In one case (R167A), the fractional decrease in z_N was greater than the decrease in q_{aLim}; but this difference could reflect a failure to achieve a limiting value of q_a. For some mutants that behaved similar to the WT (R113Q, D133Q, and R210Q), z_N was not measured and z_L was set equal to the WT value. For mutations of R207 or R210, z_L was

constrained by the voltage dependence of P_o at positive voltages as described below.

Effects of S4 Mutation on the Equilibrium Constant for Voltage Sensor Activation

Most mutations in S1–S4 shifted the P_o-V relation to more positive or negative voltages relative to the WT (Fig. 2 D), reflecting changes in the voltage sensor half-activation voltage ($V_{HC}(J)$, Table I). $V_{HC}(J)$ is a function of both voltage sensor charge (z_J) and the intrinsic stability of the activated state, represented by the zero-voltage equilibrium constant J_0 (i.e., $V_{HC}(J) = -(kT/z_J)$ $\ln(J_0)$). Thus, increases in $V_{HC}(J)$ of up to several hundred millivolts produced by mutation of potential voltage-sensing residues R213 and D153 were largely accounted for by decreases in z_J, with little change in J_0 (Table I). By contrast, mutation of either R207 or R210 in S4 increased J_0 by several orders of magnitude without changing z_J, indicating that the stability of the activated state relative to the resting state was greatly enhanced. These effects on the energetics of voltage sensor activation show that non–voltage-sensing residues in S4 have an important impact on channel function.

Log(P_o)-V relations in 0 Ca^{2+} for the WT and several mutants that increase J_0 (R207Q, R207E, and R210C) are compared in Fig. 8 A. An increase in J_0 shifts the steepest part of the curve to more negative voltages without altering its slope, as indicated by the HCA model fits (lines). This effect is most clearly demonstrated for R207Q and R207E because the steepest part of their log(P_O)-V relations can be measured, despite shifts of more than −200 mV in their position along the voltage axis relative to the WT. That charge neutralization (R207Q) and charge reversal (R207E) have virtually identical effects suggests that the removal of a positive charge at position 207 was critical for the increase in J_0. Gating current measurements confirm that mutation of R207Q enhances voltage sensor activation (Fig. 8 B) (Horrigan and Aldrich, 1999). The Q-V relation for R207Q, measured with admittance analysis (see MATERIALS AND METHODS) was shifted by −278 mV relative to the WT but is similar in shape, consistent with an increase in J_O with no change in z_J.

An important feature of the R207Q data that is reproduced by the model is the weak voltage dependence of P_o at positive voltages, evident when the P_o-V relation is plotted on a linear scale (Fig. 8 C). For R207Q at V > 0, voltage sensors are fully activated (Fig. 8 B) and P_O is limited by the weak voltage dependence of channel opening (C_4–O_4 transition in the HCA model; Fig. 3 D) determined by z_L. Therefore the P_o-V relation for R207Q is shallower than that of the WT over this voltage range.

In the case of R210C, P_O is weakly voltage dependent over a wide voltage range down to −200 mV (Fig. 8 A).
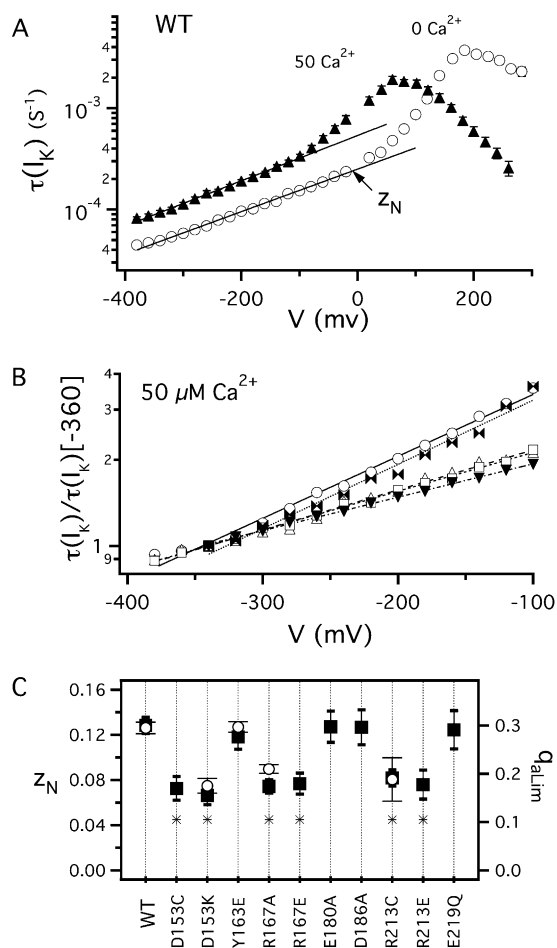
Figure 7. Voltage sensor mutations reduce the voltage dependence of channel closing. (A) Mean time constants of macroscopic I_K ($\tau(I_K)$) for WT mSlo1 in 0 Ca^{2+} (○) and 50 μM Ca^{2+} (▲) are plotted on a log scale versus voltage. The limiting exponential voltage dependence is indicated by a solid line that has a slope representing the partial charge z_N for channel closing (0 Ca^{2+}, 0.122 ± 0.002 e; 50 Ca^{2+}, 0.130 ± 0.002 e). (B) $\tau(I_K)$-V relations in 50 μM Ca^{2+}, normalized at −360 mV, for WT (○), D153K (□), R167A (▼), R213C (△), and E219Q (⋈). Lines are exponential fits. (C) z_N for WT and mutants in 50 μM Ca^{2+} (■) is compared with the limiting slope of P_o (q_{aLim}) (○). Starred symbols indicate values of z_N that are significantly different from the WT (P < 0.0001, Student's t test).

A similar observation for R210N led Diaz et. al. (1998) to conclude that R210 is a voltage-sensing residue. However several lines of evidence indicate this is not the case. First, the P_o-V relations for R210C and R207Q are virtually identical at V > 0 (Fig. 8 C), implying that the voltage sensors of R210C, like R207Q, are fully activated. Second, when the voltage range of R210C was extended to −300 mV, the voltage dependence of P_O increased (Fig. 8 A). Although we could not make measurements at sufficiently negative voltages to determine q_{aMAX}, the q_a-V relation for R210C exhibits a steepness similar to that of the WT (Fig. 8 D), consistent with the assumption that z_J is unchanged (dashed fit).
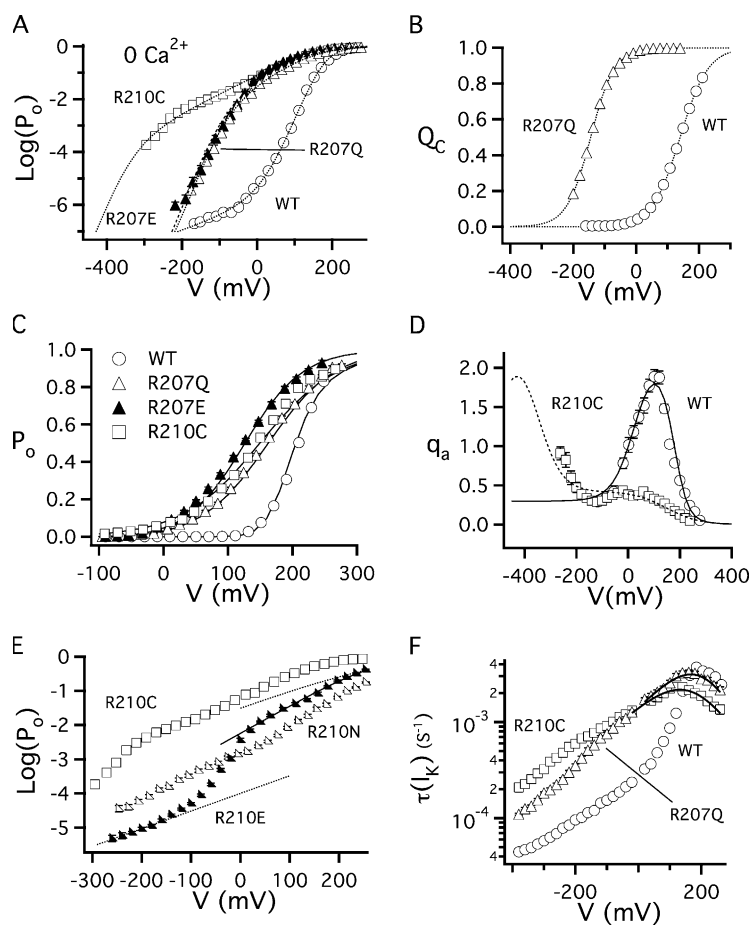
Figure 8. Effects of S4 mutation on the equilibrium for voltage sensor activation. (A) Mean $\log(P_O)$-V relations in 0 Ca^{2+} for WT(○), R207Q (△), R207E (▲), and R210C (□). Mutant curves are shifted to more negative voltages, consistent with an increase in the equilibrium constant for voltage sensor activation (J_0) in the HA model (lines, Table I parameters). (B) Normalized Q-V relations for WT and R207Q in 0 Ca^{2+} measured with admittance analysis from single experiments (see MATERIALS AND METHODS). Curves are fit with Boltzmann functions (WT: z = 0.59 e, V_h = 132 mV; R207Q: z = 0.65 e, V_h = −146 mV). (C) P_O-V relations and fits from A are plotted on a linear scale to show that mutants have a similar P_O and voltage dependence when voltage sensors are fully activated (i.e., V > 0). (D) q_a-V relations for WT and R210C in 0 Ca^{2+} together with HA model fits showing that the voltage dependence of R210C is consistent with a gating charge similar to the WT. (E) $\log(P_O)$-V relations for R210 mutants in 0 Ca^{2+} (R210C [□], R210N [◺], R210E [◣]). R210E was best fit at positive voltages by a Boltzmann function with a partial charge of 0.47 e (solid line). Dashed lines are Boltzmann functions with charge of 0.3 e, representing the value of z_L for the WT. (F) $\tau(I_K)$-V relations for WT, R207Q, and R210C. Mutant curves are fit (lines) with a bell-shaped function $\tau(I_K) = [\delta_4 + \gamma_4]^{-1}$ at potentials where voltage sensors are fully activated. δ_4 and γ_4 represent forward and backward rates for the C_4–O_4 transition in the HCA model (Fig. 3 D) and are exponentially dependent on voltage with partial charges $z(\delta_4)$ and $z(\gamma_4)$, respectively.

These observations suggest that R210C represents an extreme example of the effect represented by R207Q. That is, the voltage sensor equilibrium (J_0) for R210C is greatly increased such that the range of voltage sensor activation is shifted to extreme negative voltages, as indicated by the model fits in Fig. 8 (A and D). In this way, R210C appears weakly voltage dependent for V > −200 mV because voltage sensors are constitutively activated.

To confirm that R210 is non–voltage sensing, we examined the effects of additional mutations at this site (Fig. 8 E). Another charge-neutralizing mutation R210N exhibited reduced P_O relative to R210C, but a similar voltage dependence suggested that enhancement of voltage sensor activation does not require a cysteine residue. However a charge reversal (R210E) produced a qualitatively different effect than neutralization. First, the P_O-V relation of R210E appears less shifted than R210C and is strongly voltage dependent from −100 to +50 mV. Second, the magnitude of the P_O increase between extreme negative and positive voltages is greatly reduced relative to the WT, indicating a decrease in coupling between voltage sensor activation and channel opening (allosteric factor D). As discussed below, the P_O-V relation of R210E is consistent with a normal gat-

ing charge once changes in D are accounted for. Thus R210 is non–voltage sensing.

Voltage Sensor Activation May Increase the Charge Associated with Channel Opening

Based on the above results, we conclude that R207 and R210 are non–voltage sensing and do not contribute to z_J. However, the values of z_L determined for mutants at these positions appeared consistently larger than the WT (Table I). We do not think this represents a change in gating charge but rather a difference in the conditions under which z_L was determined. For mutants of R207 and R210, z_L was adjusted to fit the voltage dependence of P_O at positive voltages (e.g., Fig. 8 C) representing the charge to open the channel when voltage sensors are fully activated. For the WT and most mutants, z_L was determined from the voltage dependence of P_o and $\tau(I_K)$ at extreme negative voltages when voltage sensors are in the resting state. The difference in z_L might therefore be explained if the charge associated with channel opening is different when voltage sensors are in the resting or activated state. This hypothesis appears consistent with the P_o-V relation for R210E in 0 Ca (Fig. 8 E), representing the only mutant where the weak voltage dependence of P_O could be observed at both

extreme positive and negative voltages. Boltzmann functions representing WT z_L (0.3 e, dashed lines) fit the P_O-V relation of R210E at negative voltages but not at positive voltages where the data are best fit with a charge of 0.47 e (solid line). Thus it appears that z_L increases when voltage sensors are activated.

To confirm the value of z_L for mutants of R207 and R210 we also examined the voltage dependence of $\tau(I_K)$ (Fig. 8 F). When voltage sensors are fully activated, channel gating in 0 Ca^{2+} should be approximated by a two-state model (C_4–O_4) and the $\tau(I_K)$-V relation is described by bell-shaped function $\tau(I_K) = [\delta_4+\gamma_4]^{-1}$, where δ_4 and γ_4 represent the voltage-dependent forward and backward rate constants (Horrigan et al., 1999). The $\tau(I_K)$-V relations for R207Q and R210C are well fit by this function (Fig. 8 F); and the summed partial charges associated with the forward and backward rates yield values from 0.34 to 0.58 e for different mutants (R207Q, 0.51 e; R207E, 0.58 e; R210C, 0.43 e; R210E, 0.34 e; R210N, 0.48 e). These estimates are comparable to values of z_L determine from P_o (Table I), but are probably not as accurate because the data must be fit at voltages near peak $\tau(I_K)$ where neither $z(\delta_4)$ nor $z(\gamma_4)$ are well constrained.

Effects on Coupling between Voltage Sensor Activation and Channel Opening

Because decreases in the voltage dependence of P_o can be caused by decreases in allosteric coupling, we were careful to examine the effects of mutation on the coupling factor D. In most cases, large voltage-dependent increases in P_O were observed in 0 Ca^{2+}, indicating that D was unchanged. However, three mutations (R210E, E180A, and D186A) reduced D significantly (Table I). Two of these in S3 (E180A, D186A) represent relatively small changes (twofold) that have a small impact on q_{amax} (<15%). By contrast, R210E exhibited a 30% reduction in q_{amax} that we attribute entirely to a sevenfold decrease in D.

Both R210E and E180A decreased the coupling factor D without altering gating charge. This is evident by comparing the $\log(P_O)$-V relations of these mutants to the WT in 0 Ca^{2+} (Fig. 9 A). The foot of the curve for mutants and WT is superimposable, unlike mutants of potential voltage-sensing residues (Fig. 5 F), indicating that gating charge is not altered. However the magnitude of the voltage-dependent P_o increase is reduced relative to the WT, especially in the case of R210E. P_O-V relations for R210E in different $[Ca^{2+}]$ are plotted in Fig. 9 B together with fits to the WT data (dashed lines). The weak voltage dependence of R210E at both positive and negative voltages is consistent with complete activation and deactivation of voltage sensors, respectively. Between these extremes, P_o increases sharply over a 150 mV range like WT, consistent with a normal voltage sensor charge, but the magnitude of the P_o increase is

roughly 1,000-fold smaller than WT. In 0 Ca^{2+}, P_o for R210E is less than the WT at positive voltages but is ~100-fold greater than the WT at extreme negative voltages. These differences can be reproduced with the HA model (solid lines) by a sevenfold reduction in D and a 100-fold increase in L_O. The reduction in D is necessary to account for the reduced magnitude of the voltage-dependent P_o increase and also accounts for the decrease in q_{amax} (Fig. 9 C). The q_a-V relation for R210E is narrower than that of the WT but has similar steepness at negative voltages, supporting the conclusion that coupling is reduced without altering gating charge.

The ability of R210C and R210N to enhance voltage sensor activation prevented us from determining whether these mutants reduce coupling; we could not measure P_o when voltage sensors were in the resting state nor determine q_{aMAX}. The q_a-V relation for R210C can be fit with a WT value of D (Fig. 8 D) but is also consistent with a function like that describing R210E (Fig. 9 C). One reason to suspect that R210C does not alter coupling is that its P_O in 0 Ca^{2+} closely matches that of R207Q and R207E when voltage sensors are fully activated (Fig. 8 A). R207 mutants exhibit a large decrease in P_o at negative voltages, indicating a value of D similar to the WT. By the same logic, R210N may decrease coupling because P_o is reduced relative to the WT, like R210E at positive voltages. However, a decrease in the intrinsic stability of the open state (L_0) could also account for the effect of R210N on P_o.

The coupling factor D was also difficult to determine for some mutants that reduce gating charge. In the case of D186A, the data were well fit by a 50% reduction in D (Fig. 5 E and Fig. 6 E). However, a broadening of the P_O-V relation produced by a 37% decrease in z_J together with poor expression of this mutant prevented us from comparing P_o at sufficiently positive and negative voltages to assure that voltage sensors were fully activated and fully deactivated. Thus, it is conceivable that D was underestimated, in which case the impact on gating charge was also underestimated. Conversely, the value of D and impact on gating charge could have been overestimated for mutants of D153 and R213 where P_O could not be measured when voltage sensors are fully activated.

Despite uncertainty concerning the impact of D153 and R213 on allosteric coupling, there is no question that the main effect of mutating these sites is on gating charge. The broadening of P_o-V and q_a-V relations, and reduced voltage dependence of q_a and $\tau(I_K)$ (Fig. 5, B and C; Fig. 6, B and C) are all indicative of decreases in charge and cannot be reproduced by decreasing D. Likewise, large decreases in D sufficient to account for reductions in q_{aMAX} should produce obvious changes in the shape of P_o-V relation, similar to R210E, that are not observed for mutants of D153 or R213.
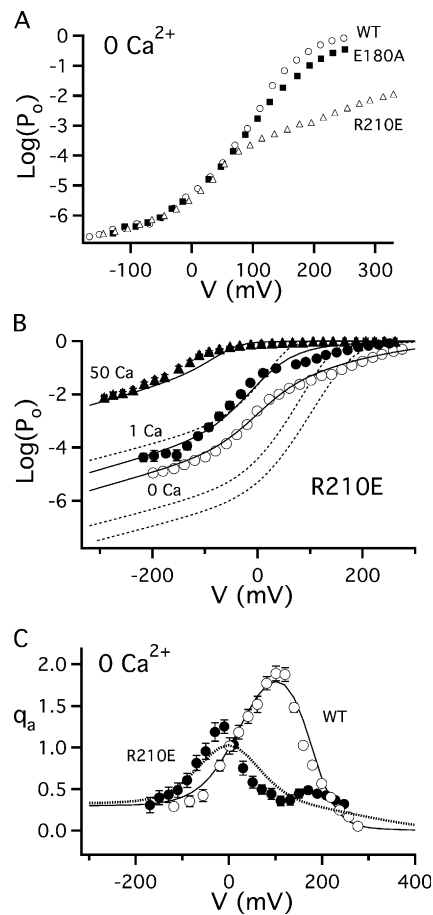
Figure 9. Effects of voltage sensor mutations on coupling. (A) Mean log(P_O)-V relations for WT ($\bigcirc$), E180A($\blacksquare$), and R210E ($\triangle$) in 0 Ca^{2+} are superimposed as in Fig. 5 F to show that mutations reduce the magnitude of the voltage-dependent P_O increase without altering the voltage sensitivity of P_O at negative voltages. (B) Mean log(P_O)-V relations for R210E in 0–50 μM Ca^{2+}. Solid lines are the fits to the HA model (Table I parameters) with the coupling factor D reduced sevenfold relative to the WT (dashed lines). (C) q_a-v relations for R210E ($\bullet$) and WT ($\bigcirc$) in 0 Ca^{2+} with HA model fits. The similar voltage dependence of the foot of these curves show that gating charge (z_J, z_L) is unchanged.

DISCUSSION

The contributions of charged residues in the S1–S4 voltage sensor domain of Slo1 to gating charge, voltage sensor stability, and channel opening are discussed below in terms allosteric models of BK channel gating and alternative mechanisms of voltage sensor activation. We also consider that many differences between BK and K_V channels may be accounted for if the resting conformation of the BK channel voltage sensor resembles the activated state in Shaker.

Voltage-sensing Residues

Our results suggest that the weak voltage dependence of BK channel activation reflects differences relative to K_V

channels in the number, movement, and position of voltage-sensing residues. S4 is the primary voltage sensor of most voltage-gated channels and is the most highly charged transmembrane segment in Slo1. However, only one out of five charged S4 residues in Slo1 (R213) contributes to gating charge. In contrast, at least four out of seven in Shaker are voltage sensing. That a small fraction of charged S4 residues are voltage sensing accounts in large part for the weak voltage dependence of BK channel gating and suggests that voltage sensor movement may be reduced. Consistent with this possibility, the contribution of individual residues to gating charge in Slo1 is less than in Shaker. Four S4 arginines in Shaker are each thought to contribute $\sim$1 e per subunit (Aggarwal and MacKinnon, 1996; Seoh et al., 1996) and at least three of these move completely through the electric field (Larsson et al., 1996; Starace and Bezanilla, 2001). By contrast, neutralization of R213 in Slo1 reduced voltage sensor charge (z_J) by only 0.30 e.

Although R213 appears to make the largest single contribution to gating charge, regions outside of S4 are also important; and it is possible that S4 is not the primary voltage sensor of BK channels. The effects of mutating D153 in S2 are nearly as large as those of R213; and the summed effects on z_T of mutating S2 and S3 residues (D153, R167, and D186) greatly exceed that of S4. Because potential voltage-sensing residues may have indirect effects on gating charge (discussed below), the relative contributions of S2, S3, and S4 to voltage sensing cannot be precisely determined. However, the 50% reduction in z_T produced by neutralizing R213 likely represents an upper limit for the direct contribution of S4. Therefore, regions outside of S4 must account for at least 50% of gating charge.

The possibility that S2 and S3 segments contribute to voltage sensing is not unique to BK channels. Neutralization of an S2 residue in Shaker (E293) has effects on gating charge comparable to any single S4 mutation (Seoh et al., 1996). Addition of negative charge at the equivalent position in Slo1 (Y163E) had no effect on voltage sensitivity, supporting the conclusion that the movement or position of the voltage sensor in the electric field differ for BK and K_V channels. Conversely, neutralization of residues in Shaker S2 and S3 corresponding to D153 and D186 in mSlo1 had no significant effects on gating charge (Seoh et al., 1996). However, the standard errors of measurements in Shaker ($\sim$1.5 e) were larger than any of the changes in z_T reported here for mSlo1. Thus, it is conceivable that residues in Shaker corresponding to D153, D186, or R167 in mSlo1 make contributions to gating charge equivalent to those in mSlo1. Indeed Seoh et al. suggested that D316 (D186 in mSlo1) might make a small contribution.

Indirect Effects of Mutation on Gating Charge
Charge-neutralizing mutations can have direct and indirect effects on gating charge. The direct effect is to

remove a charge that contributes to z_T. Indirect effects include unknown changes in voltage sensor conformation or movement that alter the fraction of the electric field traversed by unmutated residues. Voltage sensor function can be greatly perturbed by mutation without indirect effects on gating charge (e.g., R207Q, R210E). Likewise, mutations of potential voltage-sensing residues appear unlikely to cause gross disruptions in channel structure because most parameters other than gating charge were not altered (Table I). Yet indirect effects exist, because the summed decreases in z_J or z_T produced by neutralizing these residues (150% and 147%, respectively) exceed 100%, as also reported for Shaker (Aggarwal and MacKinnon, 1996; Seoh et al., 1996). Thus, our results may overestimate the direct contribution of one or more potential voltage-sensing residues to gating charge. However, non–voltage-sensing residues should be correctly identified unless mutations at such sites have direct and indirect effects that cancel out. Therefore it is important that all conserved charged residues in S1–S4 were tested and most found to be non–voltage sensing. This finding supports the conclusion that four potential voltage-sensing residues must account for the majority of gating charge.

Our conclusion that R213 and R210 demark the boundary between voltage-sensing and non–voltage-sensing arginines in S4 is supported by previous results concerning the accessibility of these positions to the cysteine-modifying reagent MTSES at −80 mV (Hu et al., 2003). R213C was modified from the internal solution, whereas R210C was modified only from the external solution. At −80 mV, the voltage sensors of R213C and R210C are in resting and activated states, respectively (Table I). Nonetheless, the observed differences in accessibility are consistent with R213 being in a position to move through the electric field and act as a voltage sensor and suggest that the non–voltage-sensing residues R210 and R207 may remain exposed to the external solution.

Voltage Sensor Stability and State-dependent Salt Bridge Interactions

Two non–voltage-sensing charged residues in S4 (R207, R210) contribute greatly to the relative stability of the resting and activated state, suggesting they participate in state-dependent interactions. The structures of K_VAP (Jiang et al., 2003) and $K_V1.2$ (Long et al., 2005a) and studies in Shaker (Papazian et al., 1995; Tiwari-Woodruff et al., 1997) indicate that salt bridge interactions occur between oppositely charged residues in the voltage sensor domain; but it is generally unknown whether such interactions depend on the activation state of the voltage sensor. A state-dependent interaction could have an impact on the equilibrium constant for voltage sensor activation (J_0) comparable to the salt bridge interaction energy. Many mutations altered

J_0 (Table I), reflecting the energetic difference between resting and activated conformations at V = 0 (i.e., $\Delta G_v = -kT\ln(J_0)$). In most cases, the change in free energy ($\Delta\Delta G_V = -kT\ln(J_0^M / J_0^{WT})$) (Fig. 10 A) was too small to draw any conclusions. However, mutations of R207 or R210 had large effects ($\Delta\Delta G_v = -2$ to -7 kcal/mol), consistent with state-dependent salt bridge interactions. Because all mutations at these sites enhanced voltage sensor activation, interaction of R207 and R210 with their unknown partner(s) is likely favored in the resting rather than the activated state (Fig. 10 B). That R207 participates in a salt bridge interaction is supported by virtually identical effects of charge neutralization and charge reversal at this site (Fig. 8 A; Fig. 10 A; R207Q, R207E).

Effects on Allosteric Coupling

Most S1–S4 mutations altered voltage sensor function (z_J, z_L, and J_0) with little impact on other aspects of gating. However, three mutations decreased the allosteric coupling (D) of voltage sensor activation to channel opening (R210E, E180A, and D186A). The effect was particularly large for R210E, representing a 4.7 kcal mol^{-1} or 60% decrease in the total coupling energy ($\Delta G_D = 4kT\ln(D)$). Coupling between the voltage sensor and gate in K_V channels is proposed to be mediated by interactions between the S4–S5 linker and the COOH-terminal end of S6, toward the cytoplasmic side of the channel (Lu et al., 2002; Long et al., 2005a). However the 210 position is unlikely to participate in such interactions because it is in the NH$_2$-terminal half of S4, external to the voltage-sensing residue R213 and probably exposed to the external solution at all times. A role of this position in allosteric coupling could perhaps be related to our finding that voltage sensor mutations alter z_L. That is, if voltage sensor conformation is influenced by channel opening, then interactions of residues in the voltage sensor domain with each other or stationary parts of the channel could depend on the state of both voltage sensor and gate, and therefore influence the energetic coupling of these processes. Experiments in Shaker (Laine et al., 2003) and KAT1 (Lai et al., 2005) as well as the structure of Kv1.2 (Long et al., 2005a,b) support the possibility that the external end of S4 might interact with S5 in the pore domain.

Gating Charge Associated with Opening Transitions

Voltage sensor activation and channel opening are generally considered distinct conformational events involving different parts of the channel (e.g., S1–S4 vs. S5–S6). Likewise, most models of voltage gating include a concerted opening transition, separate from transitions in each voltage sensor associated with activation (Bezanilla et al., 1994; Zagotta et al., 1994; Schoppa and Sigworth, 1998; Horrigan et al., 1999). However opening transitions are usually assigned a gating charge

(z_L) in apparent conflict with the idea that voltage sensor activation and channel opening are distinct. One possible explanation is that opening of the pore forces peripherally associated voltage sensor domains to move, altering their position in the electric field (Horrigan et al., 1999). In this way, opening could cause a concerted movement of gating charge without requiring that voltage sensors activate (Fig. 11 A). That is, voltage sensors may undergo different conformational changes associated with activation and channel opening.

Two observations are consistent with the voltage sensor in Slo1 acting as a source of gating charge for the opening transition. First, mutations in S2 and S4 that reduced z_J also reduced z_L (Table I). Interestingly, D186A in S3 reduced z_J but not z_L, perhaps reflecting that the voltage sensor movement associated with activation and opening are different. Second, z_L is increased when voltage sensors are activated, as indicated by the different voltage dependence of R210E at extreme positive and negative voltages (Fig. 8 E; Fig. 10 D). If channel opening moves the voltage sensor, then z_L should be sensitive to the distribution of voltage sensor charge and therefore the state of voltage sensor activation. For example, if a charged residue moves into the electric field only when voltage sensors are activated, then the contribution of that charge to z_L will likely be reduced when voltage sensors are in the resting state (Fig. 11 A). The HCA and HA models can be modified to include different values of z_L when voltage sensors are in resting ($z_L^0 = 0.3$ e) or activated ($z_L^4 = 0.46$ e) states (Fig. 10 C, Scheme I), and reproduce the R210E data

(Fig. 10 D). However, the effect is small in terms of total gating charge and has little impact on determination of gating parameters.

A previous study supports the idea that the voltage sensor moves during opening (Pathak et al., 2005). Flourophores attached to the external end of S4 in the ILT mutant of Shaker (Smith-Maxwell et al., 1998) exhibit changes in fluorescence associated with both voltage sensor activation and channel opening, events that occur over different voltage ranges in ILT. Pathak et. al. proposed that the opening component represents a cooperative movement of voltage sensors that precedes and drives opening of the gate. However, we think the simpler possibility that voltage sensor and gate move together in a single transition (e.g., Fig. 11 A) is more likely. First, the structure of Kv1.2 (Long et al., 2005a) indicates that voltage sensors in different subunits are isolated from each other. Thus, cooperative voltage sensor movement is likely to be mediated by opening of the central pore rather than direct interaction among voltage sensors. Second, over the voltage range of opening, the gating and ionic currents of ILT exhibit similar voltage dependence and kinetics, suggesting that charge movement is coincident with opening (Ledwell and Aldrich, 1999).

Mechanisms of Voltage Sensor Activation

The conformational changes underlying activation remain controversial, and several types of mechanisms have been proposed (Blaustein and Miller, 2004). Paddle-type models assert that S4 undergoes a large
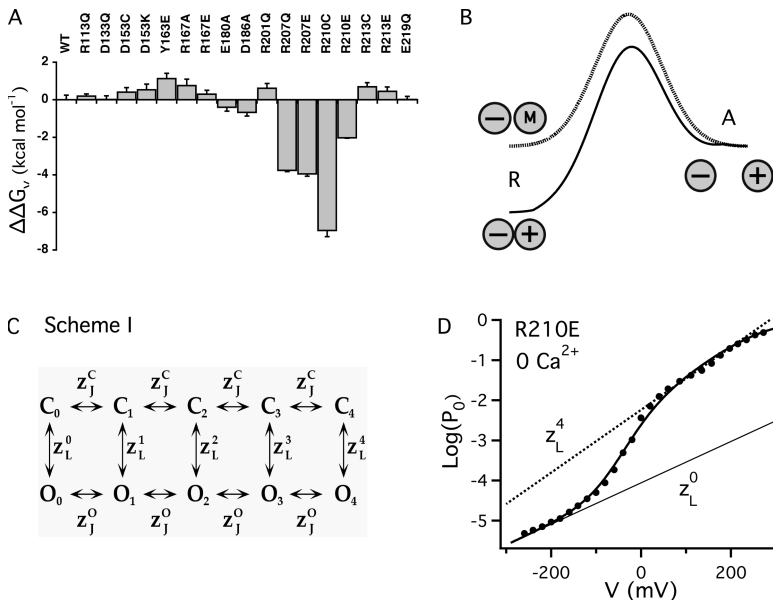

Figure 10. (A) Changes in the free energy of voltage sensor activation produced by different mutations ($\Delta\Delta G_V = -kT\ln(J_0^M / J_0^{WT})$), where the equilibrium constant J_0 is from Table I. (B) Free energy diagram for voltage sensor activation illustrates how mutation of a positively charged (+) residue representing R207 or R210 to a neutral or negatively charged residue (M) may enhance voltage sensor activation by disrupting a salt bridge interaction that normally occurs only in the resting state (R). Solid and dashed curves represent the WT and mutant, respectively. Mutation destabilizes the resting but not the activated state. (C) Scheme I represents the HCA model (Fig. 3 D) modified such that z_L increases when voltage sensors are activated. The charges for each transition are shown and the equilibrium constants are as in Fig. 3 D. z_L^i represents the C–O charge where i is the number of activated voltage sensors and $z_L^i = z_L^0 + i\Delta z$. To satisfy detailed balance the charge associated with voltage sensor activation must also be increased when channels are open ($z_J^O = z_J^C + \Delta z$). (D) Mean $\log(P_O)$-V relation for R210E in 0 Ca^{2+} is fit (solid curve) by Scheme I ($z_J = 0.59$ e, $z_L^0 = 0.3$ e, $J_0 = 1.73$, $L_o = 8.7 \times 10^{-5}$, $D = 3.1$, $\Delta z = 0.04$ e). z_L^0 was set to the WT value of z_L determined at negative voltages (0.3 e, Table I); and the fit indicates that that z_L increases to $z_L^4 = 0.46$ e when all four voltage sensors are activated. Solid and dashed lines are exponential functions with partial charges of 0.3 e and 0.46 e, respectively, to show the difference between z_L^0 and z_L^4.

movement through the lipid bilayer to translate charge across the electric field. Sliding helix models propose that aqueous crevices in the voltage sensor allow relatively small movements of S4 to translate individual voltage-sensing residues entirely through the electric field. Transporter-type models suggest that the electric field rather than voltage-sensing residues move relative to the plane of the membrane as conformational changes alter the electrical access of charged residues to the internal and external solution. Our results do not rule out any of these models but in some respects appear easier to explain in terms of a transporter-type mechanism.

Two conclusions that are strengthened by comparing Slo1 and Shaker data are that voltage-sensing residues are present outside of S4, and non–voltage-sensing residues are likely to participate in state-dependent salt bridge interactions. In Shaker, it is conceivable that reductions in gating charge upon mutation of S2 and S3 (Seoh et al., 1996) represent indirect effects on S4. However, similar findings in Slo1, where S4 does not dominate voltage sensitivity, require that some residues in S2 and/or S3 residues are voltage sensing. In addition, the summed contributions to z_T of neutralizing basic residues (R213, R167) and acidic residues (D153, D186) in mSlo1 are 73% and 74% respectively, implying that both positive and negative charges must contribute to voltage sensing, even if one or more of these residues make indirect contributions to gating charge. If a positively charged residue in S4 and negatively charged residues in S2 and/or S3 both contribute to gating charge, they must move in opposite directions through the electric field during voltage sensor activation. Such an effect seems difficult to explain strictly in terms of paddle or sliding helix mechanisms where S2/S3 and S4 must move in opposite directions relative to the membrane. However, a transporter-type mechanism would require only that voltage sensor activation decrease access of S4, S2 positive charges to the internal solution (or increase external access) and decrease access of S2, S3 negative charges to the external solution (or increase internal access). Such changes could be accomplished with relatively subtle rearrangements in the packing of the S1–S4 segments (e.g., Fig. 11 B). Although a transporter-type mechanism is useful for explaining the contributions of S2 and S3, it does not rule out alternative models of S4 movement because a combination of mechanisms is possible. For example, an outward movement of S4 might cause repacking of S2 and S3, similar to Fig.11 B, such that negative charges in these segments contribute to voltage sensing without moving inward.

Regardless of the model, the apparent contribution of positively and negatively charged residues to voltage sensing suggests that S4 moves relative to S2/S3, supporting the possibility of state-dependent inter-
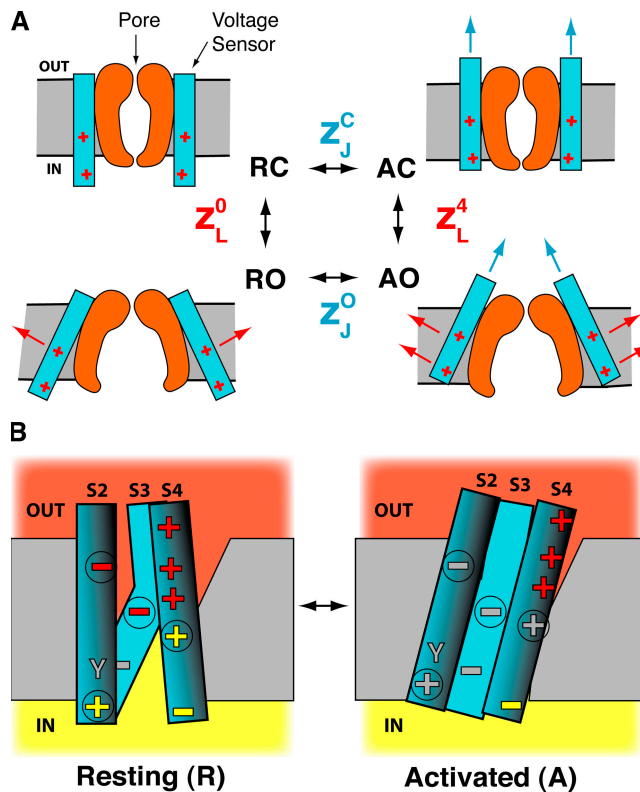
Figure 11. Mechanisms of voltage sensor activation. (A) Cartoon illustrates how voltage sensors may contribute to the gating charge associated with channel opening (z_L). The pore and voltage sensor domains for two subunits in a channel are depicted in different combinations of O/C and R/A states respectively. When all voltage sensors are in the resting state, channel opening (RC to RO) displaces peripherally associated voltage sensors through the membrane electric field, thereby moving gating charge (red arrow, z_L^O). For illustration purposes, the voltage sensor is represented by a positively charged rod that translates along its axis when activated (e.g., RC to AC, blue arrow). Activation alters the charge distribution; in this case, moving one of the voltage sensor charges into the electric field. This redistribution allows more gating charge to move upon channel opening (double red arrows) such that z_L is increased when voltage sensors are activated (i.e., $z_L^4 > z_L^O$). (B) Transporter-type mechanism of voltage sensor activation illustrates how positively and negatively charged voltages sensing residues in S2, S3, and S4 may both contribute to gating charge in mSlo1. All charged residues in S2–S4 are shown. Mutation of potential voltage-sensing residues (circled) reduce gating charge, implying that positive and negative charges must move in opposite directions through the electric field during activation. In the resting state, these positive and negative charges are shown as exposed to the internal (yellow) and external (red) solutions, through aqueous crevices, and therefore lie outside of the electric field. Upon activation, the packing of S2–S4 segments is altered such that charges are buried in the electric field, effectively moving positive charges outward and negative charge inward. Colors indicate the exposure of each residues (red, out; yellow, in; gray, buried). Non–voltage-sensing residues and positions (Y163) are shown as remaining in a constant environment.

actions between these segments. Although we find mutations in S4 greatly alter J_0, consistent with participation in state-dependent interactions, the interaction

partners for these residues have not been identified. Conversely, in Shaker, interactions between S4 and S2/S3 have been identified, but their impact on voltage sensor activation could not be defined (Tiwari-Woodruff et al., 2000). Thus, taken together, results from Shaker and Slo1 support a view of the voltage sensor as a dynamic structure whose activation involves changes in the relative position and interaction of transmembrane segments.

The Activation State of BK and K_V Channel Voltage Sensors

Differences in the distribution of S4 and S2 residues that contribute to voltage sensing in Slo1 and K_V channels provide a possible explanation for the weak voltage dependence of BK channel gating. Only one S4 residue in Slo1 is voltage sensing (R213) and the remaining S4 arginines (R201, R207, and R210) are external to this residue. In contrast, the four most external S4 arginines in Shaker are the most important voltage-sensing residues. This difference suggests that the resting conformation of Slo1 may resemble the activated state of Shaker where NH_2-terminal arginines become exposed to the external environment (Larsson et al., 1996; Baker et al., 1998). Similarly, the failure of the Y163E mutation in Slo1 to alter voltage sensitivity could be explained if the corresponding negatively charged voltage-sensing position in Shaker (E293) is moved out of the electric field upon voltage sensor activation.

The possibility that voltage sensors in BK channels are more activated than in Shaker might account for several functional differences between these channels. Activation of voltage sensors in Shaker is thought to proceed through at least one intermediate activated state based on the presence of multiple gating current components (Bezanilla et al., 1994; Zagotta et al., 1994; Schoppa and Sigworth, 1998). In contrast, gating currents in Slo1 channels are consistent with a single resting and activated state and are much faster than in Shaker (Horrigan and Aldrich, 1999). These differences and the smaller gating charge of BK channels might be explained if the BK channel resting state is equivalent to an intermediate activated state of Shaker. Partial activation might also account for the ability of BK channels, unlike Shaker, to open when voltage sensors are in the resting state (Horrigan et al., 1999).

Summary

By determining the effects on gating of mutating each conserved charged residue in S1–S4, we have narrowed the list of potential voltage-sensing residues in Slo1 to four, shown that the contribution of S4 is limited, and identified important functional roles for residues that are non–voltage sensing. Our results differ from those in Shaker, reflecting fewer voltage-sensing residues in Slo1 and a much smaller contribution of individual residues to gating charge. In K_V and Na^+ channels, some residues have been confirmed to be voltage sensing based on the ability of substituted Cys or His residues to access both internal and external solutions during voltage sensor activation (Larsson et al., 1996; Yang et al., 1996; Starace and Bezanilla, 2001). Such confirmation is unlikely in Slo1 since no residue makes a large contribution to gating charge consistent with its translation through the entire electric field. That nature has apparently chosen to reduce the voltage sensitivity of BK channels by restricting the movement of charged residues rather than reducing their number may reflect the essential role of these residues for functions other than voltage sensing. For example, effects on voltage sensor stability of mutating key arginines in S4 (R207, R210) suggest these charges cannot be eliminated without effectively locking voltage sensors in the activated state at physiological voltages. Interestingly, cyclic nucleotide-gated (CNG) channels contain many charged residues in the voltage sensor domain (Jan and Jan, 1990) but have been proposed to be constitutively activated (Tang and Papazian, 1997), and retain an effective gating charge ($z = 0.22\ e$) (Benndorf et al., 1999) comparable to that associated with channel opening in Slo1 (z_L).

REFERENCES

Aggarwal, S.K., and R. MacKinnon. 1996. Contribution of the S4 segment to gating charge in the Shaker K+ channel. *Neuron.* 16:1169–1177.

Almers, W. 1978. Gating currents and charge movements in excitable membranes. *Rev. Physiol. Biochem. Pharmacol.* 82:96–190.

Armstrong, C.M., and F. Bezanilla. 1974. Charge movement associated with the opening and closing of the activation gates of the Na channels. *J. Gen. Physiol.* 63:533–552.

Baker, O.S., H.P. Larsson, L.M. Mannuzzu, and E.Y. Isacoff. 1998. Three transmembrane conformations and sequence-dependent displacement of the S4 domain in shaker K+ channel gating. *Neuron.* 20:1283–1294.

Benndorf, K., R. Koopmann, E. Eismann, and U.B. Kaupp. 1999. Gating by cyclic GMP and voltage in the α subunit of the cyclic GMP-gated channel from rod photoreceptors. *J. Gen. Physiol.* 114:477–490.

Bezanilla, F., E. Perozo, and E. Stefani. 1994. Gating of Shaker K+ channels: II. The components of gating currents and a model of channel activation. *Biophys. J.* 66:1011–1021.

Blaustein, R.O., and C. Miller. 2004. Ion channels: shake, rattle or roll? *Nature.* 427:499–500.

Butler, A., S. Tsunoda, D.P. McCobb, A. Wei, and L. Salkoff. 1993. mSlo, a complex mouse gene encoding "maxi" calcium-activated potassium channels. *Science.* 261:221–224.

Cox, D.H., J. Cui, and R.W. Aldrich. 1997. Allosteric gating of a large conductance Ca-activated K+ channel. *J. Gen. Physiol.* 110:257–281.

Diaz, F., M. Wallner, E. Stefani, L. Toro, and R. Latorre. 1996. Interaction of internal Ba^{2+} with a cloned Ca^{2+}-dependent K^+ (hslo) channel from smooth muscle. *J. Gen. Physiol.* 107: 399–407.

Diaz, L., P. Meera, J. Amigo, E. Stefani, O. Alvarez, L. Toro, and R. Latorre. 1998. Role of the S4 segment in a voltage-dependent calcium-sensitive potassium (hSlo) channel. *J. Biol. Chem.* 273:32430–32436.

Hamill, O.P., A. Marty, E. Neher, B. Sakmann, and F.J. Sigworth. 1981. Improved patch-clamp techniques for high-resolution current recording from cells and cell-free membrane patches. *Pflugers. Arch.* 391:85–100.

Herrington, J., and R.J. Bookman. 1995. Pulse Control. University of Miami Press, Miami.

Hirschberg, B., A. Rovner, M. Lieberman, and J. Patlak. 1995. Transfer of twelve charges is needed to open skeletal muscle Na^+ channels. *J. Gen. Physiol.* 106:1053–1068.

Horrigan, F.T., and R.W. Aldrich. 1999. Allosteric voltage gating of potassium channels II. Mslo channel gating charge movement in the absence of Ca^{2+}. *J. Gen. Physiol.* 114:305–336.

Horrigan, F.T., and R.W. Aldrich. 2002. Coupling between voltage sensor activation, Ca^{2+} binding and channel opening in large conductance (BK) potassium channels. *J. Gen. Physiol.* 120:267–305.

Horrigan, F.T., J. Cui, and R.W. Aldrich. 1999. Allosteric voltage gating of potassium channels I. mSlo ionic currents in the absence of Ca^{2+}. *J. Gen. Physiol.* 114:277–304.

Hu, L., J. Shi, Z. Ma, G. Krishnamoorthy, F. Sieling, G. Zhang, F.T. Horrigan, and J. Cui. 2003. Participation of the S4 voltage sensor in the Mg^{2+}-dependent activation of large conductance (BK) K+ channels. *Proc. Natl. Acad. Sci. USA.* 100:10488–10493.

Islas, L.D., and F.J. Sigworth. 1999. Voltage sensitivity and gating charge in Shaker and Shab family potassium channels. *J. Gen. Physiol.* 114:723–742.

Jan, L.Y., and Y.N. Jan. 1990. A superfamily of ion channels. *Nature.* 345:672.

Jiang, Y., A. Lee, J. Chen, M. Cadene, B.T. Chait, and R. MacKinnon. 2002. The open pore conformation of potassium channels. *Nature.* 417:523–526.

Jiang, Y., A. Lee, J. Chen, V. Ruta, M. Cadene, B.T. Chait, and R. MacKinnon. 2003. X-ray structure of a voltage-dependent K^+ channel. *Nature.* 423:33–41.

Lai, H.C., M. Grabe, Y.N. Jan, and L.Y. Jan. 2005. The S4 voltage sensor packs against the pore domain in the KAT1 voltage-gated potassium channel. *Neuron.* 47:395–406.

Laine, M., M.C. Lin, J.P. Bannister, W.R. Silverman, A.F. Mock, B. Roux, and D.M. Papazian. 2003. Atomic proximity between S4 segment and pore domain in Shaker potassium channels. *Neuron.* 39:467–481.

Larsson, H.P., O.S. Baker, D.S. Dhillon, and E.Y. Isacoff. 1996. Transmembrane movement of the *shaker* K^+ channel S4. *Neuron.* 16:387–397.

Ledwell, J.L., and R.W. Aldrich. 1999. Mutations in the S4 region isolate the final voltage-dependent cooperative step in potassium channel activation. *J. Gen. Physiol.* 113:389–414.

Long, S.B., E.B. Campbell, and R. Mackinnon. 2005a. Crystal structure of a mammalian voltage-dependent Shaker family K^+ channel. *Science.* 309:897–903.

Long, S.B., E.B. Campbell, and R. Mackinnon. 2005b. Voltage sensor of Kv1.2: structural basis of electromechanical coupling. *Science.* 309:903–908.

Lu, Z., A.M. Klem, and Y. Ramu. 2002. Coupling between voltage sensors and activation gate in voltage-gated K^+ channels. *J. Gen. Physiol.* 120:663–676.

Neyton, J. 1996. A Ba^{2+} chelator suppresses long shut events in fully activated high-conductance Ca^{2+}-dependent K^+ channels. *Biophys. J.* 71:220–226.

Papazian, D.M., X.M. Shao, S.A. Seoh, A.F. Mock, Y. Huang, and D.H. Wainstock. 1995. Electrostatic interactions of S4 voltage sensor in Shaker K^+ channel. *Neuron.* 14:1293–1301.

Pathak, M., L. Kurtz, F. Tombola, and E. Isacoff. 2005. The cooperative voltage sensor motion that gates a potassium channel. *J. Gen. Physiol.* 125:57–69.

Schoppa, N.E., and F.J. Sigworth. 1998. Activation of Shaker potassium channels. III. An activation gating model for wild-type and V2 mutant channels. *J. Gen. Physiol.* 111:313–342.

Seoh, S.A., D. Sigg, D.M. Papazian, and F. Bezanilla. 1996. Voltage-sensing residues in the S2 and S4 segments of the Shaker K^+ channel. *Neuron.* 16:1159–1167.

Sigg, D., and F. Bezanilla. 1997. Total charge movement per channel. The relation between gating charge displacement and the voltage sensitivity of activation. *J. Gen. Physiol.* 109:27–39.

Smith-Maxwell, C.J., J.L. Ledwell, and R.W. Aldrich. 1998. Uncharged S4 residues and cooperativity in voltage-dependent potassium channel activation. *J. Gen. Physiol.* 111:421–439.

Starace, D.M., and F. Bezanilla. 2001. Histidine scanning mutagenesis of basic residues of the S4 segment of the shaker K^+ channel. *J. Gen. Physiol.* 117:469–490.

Stefani, E., M. Ottolia, F. Noceti, R. Olcese, M. Wallner, R. Latorre, and L. Toro. 1997. Voltage-controlled gating in a large conductance Ca^{2+}-sensitive K^+ channel (hslo). *Proc. Natl. Acad. Sci. USA.* 94:5427–5431.

Tang, C.Y., and D.M. Papazian. 1997. Transfer of voltage independence from a rat olfactory channel to the *Drosophila* ether-a-go-go K^+ channel. *J. Gen. Physiol.* 109:301–311.

Tiwari-Woodruff, S.K., M.A. Lin, C.T. Schulteis, and D.M. Papazian. 2000. Voltage-dependent structural interactions in the Shaker K^+ channel. *J. Gen. Physiol.* 115:123–138.

Tiwari-Woodruff, S.K., C.T. Schulteis, A.F. Mock, and D.M. Papazian. 1997. Electrostatic interactions between transmembrane segments mediate folding of Shaker K^+ channel subunits. *Biophys. J.* 72:1489–1500.

Wallner, M., P. Meera, and L. Toro. 1996. Determinant for β-subunit regulation in high-conductance voltage-activated and Ca^{2+}-sensitive K^+ channels: an additional transmembrane region at the N terminus. *Proc. Natl. Acad. Sci. USA.* 93:14922–14927.

Yang, N., A.J. George, and R. Horn. 1996. Molecular basis of charge movement in voltage-gated sodium channels. *Neuron.* 16:113–122.

Zagotta, W.N., T. Hoshi, and R.W. Aldrich. 1994. Shaker potassium channel gating. III: Evaluation of kinetic models for activation. *J. Gen. Physiol.* 103:321–362.

Zhang, M., J. Liu, and G.N. Tseng. 2004. Gating charges in the activation and inactivation processes of the HERG channel. *J. Gen. Physiol.* 124:703–718.